26 October 2016: Final revisions, AA and JWH

Zonation of sulfate and sulfide minerals and isotopic composition in the Far Southeast porphyry and Lepanto epithermal Cu-Au deposits, Philippines

J.W. Hedenquist [1], A. Arribas R. [2, 3], M. Aoki

Geological Survey of Japan, 1-1-1 Higashi, Tsukuba 305-8567, Japan

present addresses:

[1] Department of Earth and Environmental Sciences, University of Ottawa

[2] Department of Earth and Environmental Sciences, University of Michigan

[3] Faculty of International Resource Science, Akita University

Revision to: Resource Geology

Running title: Far Southeast-Lepanto porphyry-epithermal deposits

Keywords: porphyry, epithermal, S-isotopic composition, alunite, anhydrite, chalcopyrite, pyrite, enargite

Abstract:
The world-class Far Southeast (FSE) porphyry system, Philippines, includes the FSE Cu-Au porphyry deposit, the Lepanto Cu-Au high-sulfidation deposit and the Victoria-Teresa Au-Ag intermediate sulfidation veins, centered on the intrusive complex of dioritic composition. The Lepanto and FSE deposits are genetically related and both share an evolution characterized by early stage-1 alteration (deep FSE potassic, shallow Lepanto advanced argillic-silicic, both at ~1.4 Ma), followed by stage-2 phyllic alteration (at ~1.3 Ma); the dominant ore mineral deposition within the FSE porphyry and the Lepanto epithermal deposits occurred during stage 2. We determined the chemical and S-isotopic composition of sulfate and sulfide minerals from Lepanto, including stage-1 alunite (12 to 28 permil), aluminum-phosphate-sulfate (APS) minerals (14 to 21 permil) and pyrite (-4 to 2 permil), stage 2-sulfides (mainly enargite-luzonite and some pyrite, –10 to –1 permil), and late stage-2 sulfates (barite and anhydrite, 21 to 27 permil). The minerals from FSE include stage-2 chalcopyrite (1.6 to 2.6 permil), pyrite (1.1 to 3.4 permil) and anhydrite (13 to 25 permil). The whole rock S-isotopic composition of weakly altered syn-mineral intrusions related is 2.0 permil.

Stage-1 quartz-alunite-pyrite of the Lepanto lithocap, above ~650 m elevation, formed from acidic condensates of magmatic vapor at the same time as hypersaline liquid formed potassic alteration (biotite) near sea level. The S-isotopic composition of stage-1 alunite-pyrite record temperatures of ~300-400^{o}C for the vapor condensate directly over the porphyry deposit; this cooled to <250^{o}C as the acidic condensate flowed to the NW along the Lepanto fault where it cut the unconformity at the top of the basement. There are APS minerals with Sr, Ba, Ca at the base of the advanced argillic lithocap over the porphyry deposit, as cores to stage-1 alunite. These APS minerals show a large degree of chemical and S-isotopic heterogeneity within and between samples, based on back-scattered electron and ion microprobe results. The variation in S-isotopic values in these finely banded alunite and APS minerals (16 permil), as well as that of pyrite (6 permil) was due largely to changes in temperature, and perhaps variation in redox conditions (average ~2:1 H_2S/SO_4). Such fluctuations could have been related to fluid pulses caused by injection of

mafic melt into the diorite magma chamber, supported by mafic xenoliths hosted in diorite of an earlier intrusion.

The S-isotopic values of stage-2 minerals indicate temperatures as high as 400°C near sea level in the porphyry deposit, associated with a relatively reduced fluid (~10:1 H_2S/SO_4) responsible for deposition of chalcopyrite. Both stage-1 and particularly stage-2 fluids were relatively oxidized in the Lepanto lithocap, with a H_2S/SO_4 ratio of ~4. The oxidation resulted from cooling, which was caused by boiling during ascent and then dilution with steam-heated meteoric water in the lithocap. This cooling also resulted in the sulfidation state of minerals increasing from chalcopyrite stability in the porphyry deposit to that of enargite in the lithocap-hosted high-sulfidation deposit. The temperature at the base of the lithocap during stage 2 was ≥300°C, cooling to <250°C within the main lithocap, and ~200°C toward the limit of the Lepanto orebody, ~2 km NW of the porphyry deposit. Approximate 300 and 200°C isotherms, estimated from S-isotopic and fluid-inclusion temperatures during stage 1 and stage 2, shifted towards the core of the FSE porphyry deposit with time. This general retreat in isotherms was more than 500 m laterally within Lepanto and 500 m vertically within FSE as the magmatic-hydrothermal system evolved and collapsed over the magmatic center. During this evolution, there is also evidence recorded by large S-isotopic variations in individual crystals for sharp pulses of higher temperature, relatively reduced fluid injected into the porphyry deposit.

1. Introduction

Bodies of leached residual quartz, with alteration halos of advanced argillic minerals including alunite, kaolinite, dickite, pyrophyllite and diaspore, host high-sulfidation epithermal gold deposits around the world (Steven and Ratté, 1960; Urashima et al., 1981, Arribas, 1995, Sillitoe, 1999). Magmatic vapors condense at shallow (<1 km) depth to form acidic solutions that leach the volcanic host rocks (Ransome, 1907; Hedenquist and Taran, 2013). In this environment, silicic and advanced argillic alteration hosted by a stratigraphic horizon is called a lithocap (Sillitoe, 1995); although lithocaps as well as their structural feeder zones may be subsequently mineralized with copper sulfides and gold, many lithocaps are barren. These zones of advanced argillic alteration are integral parts of mineralized porphyry systems (Sillitoe, 2010), and where preserved from erosion, the presence of such hypogene advanced argillic alteration indicates the potential for a porphyry deposit at depth.

The Far Southeast (FSE) porphyry system is located in the Mankayan mineral district of northern Luzon, Philippines (Hedenquist et al., 1998). The Lepanto high-sulfidation Cu-Au deposit is elongate along the Lepanto fault, NW of the surface projection of the FSE porphyry deposit; the Victoria-Teresa intermediate-sulfidation vein complex (Claveria, 2001) lies ~500-1000 m south of FSE (Fig. 1). This is one of the richest mineral districts in the southwest Pacific, both in terms of proven and potential economic value as well as abundance and diversity of hydrothermal mineralization. Following early mining, first by the Ingorots during the Ming dynasty and then in Spanish colonial time in the 19th century, the Lepanto epithermal deposit was mined underground by the Lepanto Consolidated Mining Company (LCMC); this took place initially from 1936 until WWII, when Mitsui Mining operated the mine, and then again by LCMC from 1948 to 1996. The total production from gold-rich enargite ore was 36.3 Mt at 2.9 wt% Cu, 3.4 g/t Au and 14 g/t Ag, with 0.74 Mt Cu, 92 t (2.95 Moz) Au and 393 t Ag recovered (Chang et al., 2011). The FSE porphyry ore body (Concepción and Cinco, 1989) was discovered in 1980 by the second hole drilled from surface at ~1400 m elevation, to a depth of ~1100 m (Chang et al.,

2011). This followed a proposal that there should be a porphyry deposit at depth associated with the Lepanto high-sulfidation Cu-Au deposit (Sillitoe, 1983). The deposit was defined with nearly 50 km of drilling in over 85 holes, most from underground, up to 1996. A joint venture between LCMC and Gold Fields recently conducted a 102-km drill program of 98 holes from the 700 m level (mL) of the Lepanto mine. This study confirmed an inferred resource of 892 Mt at grades of 0.7 g/t Au and 0.5 wt% Cu, equivalent to 19.8 Moz Au and 4.6 Mt Cu between levels of 500 m and –400 m elevation (Fig. 2; Gaibor et al., 2013). The Victoria-Teresa epithermal veins were discovered in 1995, had an initial resource estimate of 11 Mt at 7.3 g/t Au (2.6 Moz Au), and are still being mined.

Epithermal mineralization of high-sulfidation style at Lepanto is hosted by an advanced argillic lithocap; its base is at ~650 m elevation over potassic alteration of the deeper porphyry deposit, and rises to ~900 m elevation to the NW, with upper extent as high as the ~1100 mL (Fig. 2). Dating of alunite in the lithocap and hydrothermal biotite of the porphyry deposit indicate the same age, ~1.4 Ma (Arribas et al., 1995a). Stage-1 potassic alteration of the FSE deposit was overprinted by stage-2 white mica (phyllic) alteration, with much of the copper and gold of the porphyry deposit precipitated during the stage-2 overprint (Hedenquist et al., 1998). The average radiometric ages of the white mica are younger, at ~1.3 Ma. The fluid related to stage-2 white mica alteration is argued to have ascended to the lithocap and flowed laterally to the NW, depositing enargite and gold subsequent to the leaching event of stage 1 (Mancano and Campbell, 1995; Hedenquist et al., 1998), forming the Lepanto deposit.

We studied the mineralogy and S-isotopic composition of sulfide and sulfate minerals of the porphyry deposit and along >2 km of the Lepanto lithocap, proximal to distal, including the halo of advanced argillic alteration to the silicic body (stage 1) and silicic-hosted enargite ore (stage 2). The ore minerals at Lepanto consist mainly of enargite deposited in fractures and breccias that post-date formation of the advanced argillic alteration (Fig. 3; Hedenquist et al., 1998; Claveria, 2001); there is also luzonite and minor chalcopyrite plus various gold- and silver-bearing minerals. Alunite and aluminum phosphate-sulfate (APS) minerals of the alunite supergroup are characteristic of advanced

argillic alteration (Meyer and Hemley, 1967; Hemley et al., 1969; Stoffregen and Alpers, 1987; Aoki, 1991), and their isotopic composition, including O, H and S, has been used to help constrain formation conditions (Rye et al., 1992; Arribas et al., 1995b, Deyell et al., 2005a, b). These minerals are common at Lepanto, and in addition to their O and H isotopic variation (Hedenquist et al., 1998), also show distinctive compositional zoning that has been interpreted to indicate proximity to the high-temperature source of intrusions associated with the FSE porphyry deposit (Chang et al., 2013). In addition to the epithermal mineralogy, we also examined the chalcopyrite, pyrite and anhydrite of the underlying porphyry deposit that are largely associated with white mica (phyllic) alteration of stage 2. We discuss the variations in S-isotopic composition across this magmatic-hydrothermal system and the implications for the evolution of the hydrothermal system, from proximal porphyry to distal epithermal environments, and from early stage-1 alteration to later stage-2 mineralization that dominated metal deposition.

2.0 Geology

Gonzalez (1959), Sillitoe and Angeles (1985), Concepción and Cinco (1989) and Garcia (1991) mapped and studied the Mankayan district. Here we present an overview of the geology relevant to this study, incorporating the results of recent mapping by P.N. Dunkley (2015) that have clarified the volcanic stratigraphy and related intrusive history in the FSE and Lepanto area.

From oldest to youngest, there are five principal lithologic units in the district, exposed by river erosion (Fig. 1), including: the basal basaltic Lepanto volcanic unit; the Bagon gabbro-diorite-tonalitic batholith; the epiclastic Balili volcaniclastic unit; and the Imbanguila and Bato pyroclastic units and related intrusions of dacite to andesite composition. Much of the porphyry deposit is hosted by an intrusive complex of diorite and dacite intrusions, and was cut locally by phreatomagmatic breccia pipes that formed late in the history of the hydrothermal system.

The Lepanto volcanic unit forms a basement to the district and comprises a thick

sequence of basaltic pillow lavas with hyaloclastites and volcaniclastic rocks, with an Upper Eocene – Lower Oligocene age for the upper part of the Lepanto volcanic unit (Dunkley, 2015). The Bagon tonalite-diorite-gabbro complex, located to the west, intruded the Lepanto volcanic unit late in the deposition of the Lepanto sequence. The Oligocene to mid Miocene Balili volcaniclastic unit unconformably overlies the Lepanto volcanic unit, and consists of epiclastic andesitic breccias and conglomerates with minor volcanic sandstones and pebbly sandstones.

The Pleistocene Imbanguila and Bato dacitic pyroclastic units form an extensive cover sequence, with ages of ~1.8 to 2.2 and ≤1.5 Ma, respectively (Arribas et al., 1995a; Dunkley, 2015); the latter includes deposits of local phreatomagmatic eruptions from diatremes that are well exposed on the surface and in drill core. The Imbanguila unit locally contains mafic xenoliths in outcrops of porphyritic diorite (Dunkley, 2015). Bato volcanic products are associated with several slightly eroded domes south of the FSE deposit. Quartz diorite and andesite to dacite intrusions (referred to as the FSE intrusion complex; Dunkley, 2015) that cut the young pyroclastic cover sequences are similar in composition to the volcanic units (Hedenquist et al., 1998); they were intruded to ~300 m elevation in the porphyry deposit, and are interpreted to be related to the timing of early potassic alteration (~1.4 Ma; Arribas et al., 1995a). The intrusions may have been associated with the Bato phase of volcanism, with hornblende from the matrix of a phreatomagmatic unit in the Lepanto vicinity dated at 1.43 ± 0.21 Ma (Arribas et al., 1995a).

Secondary structures splay from the main Mankayan fault, a strand of the Philippine fault, and are oriented NW and WNW across the Lepanto – FSE area (Fig. 1). The Lepanto fault is the principal structure that controlled the location of the main Lepanto ore body but cannot be traced at surface through the Pleistocene volcanic cover in the area of the FSE ore body (P.N. Dunkley, pers. commun., 2015). Rather, the ~E-W Imbanguila fault zone matches the axis of the FSE deposit and can be traced at the surface (Dunkley, 2015).

3.0 Alteration and Mineralization

3.1 Stage-1 alteration

Potassic alteration, preserved below ~400 m elevation (Fig. 2), consists of biotite-magnetite and minor K-feldspar and is centered on quartz diorite porphyry intrusions. K-Ar ages of the biotite are 1.41±0.05 Ma (n=6; Arribas et al., 1995a). Vitreous, anhedral quartz veins associated with this early stage-1 alteration contain vapor-rich and hypersaline liquid inclusions with homogenization temperatures of ~550°C, with salinities of 50 to 55 wt% NaCl equiv., indicating lithostatic pressure estimates of ~500 b near sea level, with paleosurface at 1500-2000 m elevation (Hedenquist et al., 1998).

Advanced argillic alteration formed over the top of the porphyry deposit and consists of residual quartz and a halo of quartz-alunite-pyrite (Fig. 3) plus variable assemblages of kaolinite, dickite, pyrophyllite and diaspore. The alunite has been dated at 1.42±0.08 Ma (n=5), i.e., synchronous with the underlying potassic alteration (Arribas et al., 1995a) and is thus part of the early stage 1, representing a coupled vapor and hypersaline liquid, respectively (Hedenquist et al., 1998). Where alunite is dominant over kaolinite, dickite, diaspore, and pyrophyllite, and the matrix is quartz-rich, we use the term quartz-alunite-pyrite alteration, to distinguish this alteration style from deeper occurrences of pyrophyllite ± white mica ± kaolinite (Hedenquist et al., 1998; Z. Chang, pers. commun., 2015). The lower limit of extensive quartz-alunite-pyrite alteration is ~650 m elev., although such alteration occurs as deep as sea level, restricted to zones along fractures (Gaibor et al., 2013).

Quartz-alunite-pyrite of stage 1 and a core of more completely leached residual quartz (silicic) alteration extends WNW ~4 km from the porphyry (Fig. 1) along the unconformable contact of the Imbanguila pyroclastic unit with the underlying basaltic basement of the Lepanto volcanic unit, forming a lithocap (Fig. 2). The lithocap was localized by the Lepanto fault (Gonzalez, 1959), which has a steep dip to the NE and served as a feeder zone, causing the strong WNW elongation along with other faults. Silicic alteration and particularly the halo of quartz-alunite are well developed at the surface (with pyrite largely oxidized), where the Lepanto fault and fault splays are exposed, e.g., at the Spanish workings, the type locality for the sulfosalt mineral luzonite, which is a

dimorph of enargite. Outboard of the quartz-alunite-pyrite zone, notably where it flares along the unconformity to form a lithocap, the lateral or upper and lower contacts of quartz-alunite grade into halos of kaolinite ± dickite (Chang et al., 2011), then to chlorite or montmorillonite, depending on host rock (basement or dacite, respectively; Gonzalez, 1959). Stage-1 quartz-alunite-pyrite (advanced argillic) alteration is largely devoid of copper sulfides, and in outcrop contains <50 ppb Au (Chang et al., 2011).

3.2 Stage-2 alteration

Stage-1 potassic alteration of the FSE porphyry deposit is overprinted by stage-2 phyllic alteration of chlorite-white mica with hematite replacing magnetite, and veins of euhedral quartz that locally fill reopened stage-1 anhedral quartz veins. These euhedral quartz veins contain anhydrite-white mica-pyrite ± chalcopyrite ± bornite (Fig. 4a-c) and have bleached halos of sericite (the historic term used for white mica). Fluid inclusions in quartz near sea level provide evidence for boiling on inception of fracturing events (T_h = 350^{o}C, 5 wt% NaCl equiv), and indicate a hydrostatic depth of ~1500-2000 m below the paleowater table, consistent with the estimate of the paleosurface from the potassic stage and other constraints (Shinohara and Hedenquist, 1997; Hedenquist et al., 1998). Illite separated from the halos of white mica and earlier chlorite-white mica (sericite) alteration has an age range of 1.37 to 1.22 Ma with errors of ±0.04 to 0.10 m.y. (average 1.30±0.07 Ma, n=10; Arribas et al., 1995a). The white mica is locally associated with pyrophyllite on the margins of the porphyry and at shallower depths, with evidence for deeper occurrences along structures (Hedenquist et al., 1998; Gaibor et al., 2013, Z. Chang, pers. commun., 2015).

3.3 Stage-2 mineralization

A majority of the porphyry Cu-Au ore was deposited during the stage-2 euhedral quartz vein development (Hedenquist et al., 1998); anhydrite is variable in these and earlier veins, associated with chlorite-white mica alteration (Fig. 4). Chalcopyrite ± bornite replaces earlier pyrite (Fig. 4a, b), followed by conversion of some bornite to chalcocite,

digenite and/or covellite (Fig. 4c). Fine (<10-20 μm) blebs of gold (8-15 wt% Ag), krennerite and petzite are present within or on the margins of bornite, and elemental spikes from laser ablation-inductively coupled plasma mass spectrometry analyses indicate these minerals also occur as ~1 μm inclusions; these inclusions may have exsolved from bornite on cooling within the porphyry deposit (Bunce et al., 2015).

Cross-cutting relations indicate that ore minerals in the epithermal deposit are younger than stage-1 residual quartz and quartz-alunite-pyrite (Fig. 3a). An episode of Cu mineralization (stage 2a) occurs in an assemblage of euhedral pyrite-enargite-luzonite. In the principal ore zone along the Lepanto fault, repeated periods of brecciation were followed by deposition of sulfide minerals in the matrix, particularly enargite (Fig. 3b). Stage 2b gold occurs in microfractures that cut enargite ± luzonite, accompanied by tetrahedrite, chalcopyrite and sphalerite plus telluride and selenide minerals (Gonzalez, 1956; Tejada, 1989; Claveria and Hedenquist, 1994; Claveria, 2001). Anhydrite and barite gangue minerals were deposited after enargite, followed by late vug-filling quartz and dickite. Enargite-hosted fluid inclusion data (Mancano and Campbell, 1995) indicate that their homogenization temperature and salinity decrease with increasing distance of enargite samples from the porphyry (maximum T_h decreasing from 294 to 196°C, with average salinity decreasing from ~3.2 to 1.7 wt% NaCl equiv., respectively), over a distance of ~2 km (Fig. 2; see below).

The principal host of epithermal enargite and gold ore is silicic alteration (Fig. 3b), which starts at ~650 m elevation on the upper NW margin of the FSE body, and extends for ~2 km to the WNW along the Lepanto fault, with the top of enargite rising to ~1150 m elevation (Fig. 2), largely hosted by silicic alteration (Hedenquist et al., 1998; Chang et al., 2011). The silicic body has a halo of quartz-alunite-pyrite alteration, which extends for another 2 km to the NW (Fig. 1), with silicic alteration restricted to narrow fractures. Quartz-alunite-pyrite is supergene oxidized and is only weakly anomalous in gold where it outcrops (12 to 49 ppb Au), except where cut by narrow silicic zones along fractures, which can contain up to a few ppm Au (Chang et al., 2011).

The Lepanto fault (Fig. 1) is strongly brecciated (Fig. 3b) due to syn-mineral

movement and hosts ~70% of the epithermal ore in a zone up to ~50 m wide, called the Main Ore Body (Garcia, 1991). The balance of the mineralization occurs adjacent to the fault along the silicic lithocap, mostly in ~E-W branch veins that cut the footwall and, to a lesser extent, hanging wall (Fig. 1). As with the silicic lithocap, the base of the enargite body increases in elevation, from ~700 to 1000 m as the unconformity between the basement vocaniclastic units and dacite of the Imbanguila Fm rises to the WNW with increasing distance from the porphyry (Fig. 2; Garcia, 1991). The vertical extent of enargite ore along the Lepanto fault is typically 100 to 200 m, extending downward from the local level of the unconformity.

4. Results

4.1 Sulfate mineralogy

The alunite group minerals in the Lepanto lithocap contain K, Na, and/or Ca as endmember alunite, natroalunite and huangite, with formula $(A)Al_3(SO_4)_2(OH)_6$, where A is K, Na or $Ca_{0.5}$, respectively. There is complete solid solution between the Na and K as well as Na and Ca endmembers, with a wide miscibility gap occurring between the K and Ca endmembers (Li et al., 1992); the composition of minamiite (now known as natroalunite 2C) is $(Na,Ca_{0.5}K)Al_3(SO_4)_2(OH)_6$. The aluminum phosphate isostructural mineral is crandallite, $(CaAl_3(PO_4)(PO_3\ OH)(OH)_6)$ in the plumbogummite group, and has complete solid solution with alunite.

The most common aluminum-phosphate-sulfate (APS) minerals at Lepanto are woodhouseite, $CaAl_3(SO_4)(PO_4)(OH)_6$ (Fig. 5a), and svanbergite, $SrAl_3(SO_4)(PO_4)(OH)_6$ (Fig. 5c), members of the beudantite group. These APS minerals are typically rimmed by banded intergrowths of alunite and natroalunite (Figs. 5-7), as observed in advanced argillic lithocaps elsewhere. Associated with APS minerals and alunite overgrowths are small inclusions of diaspore (Fig. 5a), as well as trace amounts of pyrophyllite, zunyite, quartz, and, locally, tourmaline (in drillcore from U80-23). Over the top of the FSE deposit, woodhouseite is preserved as euhedral crystals with epitaxial overgrowths of alunite and natroalunite (Fig. 5b). Further from the porphyry deposit to the northwest, APS minerals

typically show strong corrosion, with replacement by alunite and natroalunite (Fig. 5c). The most distal occurrence of advanced argillic alteration sampled is located ~4 km NW of the surface projection of the porphyry deposit; here only weakly zoned alunite and natroalunite occur in the lithocap, without evidence for APS minerals (Fig. 5d).

In addition to alunite and APS minerals, which formed with advanced argillic alteration of stage 1, prior to enargite deposition (Fig. 3a), barite and anhydrite are also present in the epithermal deposit, as gangue minerals deposited after enargite of stage 2. Anhydrite is also a common mineral in stage-2 euhedral quartz veins of the deeper porphyry deposit (Fig. 4a, c), associated with white mica alteration and chalcopyrite-bornite deposition (Fig. 4b, c; Concepción and Cinco, 1989; Imai, 2000; Bunce, 2015); Gaibor et al. (2013) also report anhydrite with quartz-magnetite veins related to deep potassic alteration of stage 1, although it is not known if the anhydrite is present in reopened veins.

4.2 Compositional zoning of alunite and APS minerals

The APS minerals in the Lepanto lithocap are preserved in the cores of elongate alunite crystals (Fig. 5a), and show significant chemical variation between samples, as well as zonation within individual crystals. Sample U80-23-66' (Fig. 6) has zoned crystals up to 50-μm in size of woodhouseite that contains Sr, as well distinctly euhedral cores that are rich in Ba and Pb. There is a thin P- and Ca-rich euhedral rim indicating that woodhouseite deposited after the initial zone of alunite, although this second growth contains low Ba and Pb. As there is no evidence of dissolution of the core, it appears that K-Na-alunite began to precipitate followed by a brief return to APS deposition before a resumption of alunite growth. A sample 2 m higher in this drill core (U80-23-61') contains an APS mineral with a Ba-rich core, analogous to woodhouseite.

Electron microprobe images (Fig. 6) across growth-banded crystals indicate that svanbergite occurs as a core to woodhouseite, with some bands of woodhouseite being Pb-rich. Although trace amounts of Sr are incorporated into rims of alunite, Pb and P are not present. Chang et al. (2011) also discuss the compositions of these minerals.

4.3 S-isotopic composition of sulfide and sulfate minerals

The S-isotopic composition of sulfate and sulfide minerals (Appendix Table 1; Fig. 8) in the Lepanto lithocap, as well as samples from FSE drill core, were determined by conventional analytical techniques using KIBA reagent at the Geological Survey of Japan (Sasaki et al., 1979). Additional samples of coexisting sulfides and anhydrite from FSE drill core were collected by micro-drill (Bunce, 2015) and analyzed at the University of Ottawa, using a Continuous Flow-Isotope Ratio Mass Spectrometer after volatilization at 1800°C. The whole-rock S isotopic composition of two least-altered samples of Imbanguila diorite intrusion collected at the surface (Appendix Table 1) were also analyzed by this method. Both methods report an error of ±0.2 permil. Ion microprobe analysis of two samples with woodhouseite, alunite, anhydrite and pyrite from over the FSE ore body was conducted using the SHRIMP at Australian National University. Error for ion probe analysis is quoted at ±2 permil $\delta^{34}S$ for sulfur isotope values of sulfide and sulfate minerals; the lower sulfate contents of the woodhouseite are associated with ±3 permil $\delta^{34}S$ error.

Stage-1 alunite was sampled from the quartz-alunite-pyrite zone adjacent to the Main Ore Body in underground workings, and from structures cutting both footwall and hanging wall (Fig. 2; Appendix Table 1). Sulfide minerals from the same hand sample, mainly disseminated stage-1 pyrite in quartz-alunite-pyrite alteration, were also sampled and analyzed. Stage-2 enargite and pyrite were collected (Mancano and Campbell, 1995) from the Main Ore Body, with some samples containing sulfate minerals (Appendix Table 1). Vug-filling barite and anhydrite gangue, both of stage 2 and precipitated on enargite, were also analyzed. Anhydrite and intergrown pyrite and/or chalcopyrite, both of stage 2, were collected from FSE drill core, beneath the quartz-alunite-pyrite zone (Fig. 2).

Stage-1 pyrite from quartz-alunite-pyrite in the lithocap has $\delta^{34}S$ values that range from -11.8 (distal) to 2 permil (over the porphyry), with most values from -4 to -0.5 permil $\delta^{34}S$ (Appendix Table 1; Fig. 8). Stage-1 alunite in the lithocap, at and above the 900 m level, ranges from 13.4 to 27.0 permil $\delta^{34}S$, with most $\delta^{34}S$ values between 21 and 24 permil. Below this level over the FSE deposit, from the 680 to 870 m level, alunite $\delta^{34}S$

values range between 9 and 28 permil, including results from ion probe analysis; most values are 13 to 24 permil, lower than the typical values from the 900 to 1070 m level (Fig. 8).

Stage-2 sulfides were analyzed from 530 to –160 m elevation, within the FSE deposit (Fig. 2), including pyrite with $\delta^{34}S$ values between 1.0 and 3.4 permil, and chalcopyrite with values of 1.6 to 2.6 permil (the latter from 250 to –30 m elevation). The anhydrite that is intergrown with sulfides has $\delta^{34}S$ values of 13.2 to 24.4 permil (all but three values ≤21.5 permil) up to the 680 m level. At ≥700 m elevation, in the portion of the Lepanto deposit nearest to FSE, stage-2 anhydrite has values of 21.7 to 27.3 permil. Further to the NW in the Lepanto deposit, stage-2 sulfate gangue is largely barite, with $\delta^{34}S$ values of 20.8 to 23.0 permil at ≥1030 m level (Fig. 2; Appendix Table 1).

Stage-2 enargite has $\delta^{34}S$ values that vary from –9.7 to -0.5 permil (Appendix Table 1), with six of 21 enargite samples (including one luzonite) lighter than –5.0 permil, scattered from 700 to 1100 m levels, and all but the luzonite in the Main Ore Body (Fig. 2). Of the five stage-2 pyrite crystals intergrown with enargite, the pyrite is 0.2 to 2.3 permil heavier than the enargite in the same sample. Enargite is expected to have a fractionation factor similar to that of sphalerite due to their structural similarities (R. Seal, pers. commun., 2015). At 250°C, the approximate enargite homogenization temperatures where intergrown with pyrite (Appendix Table 1), the fractionation factor for pyrite and sphalerite, $\Delta^{34}S_{pyrite\text{-}sphalerite}$, is 1.1 permil, equal to the average $\Delta^{34}S_{pyrite\text{-}enargite}$ of 1.1 permil (0.4 to 2.3 permil average, n=5; Appendix Table 1).

4.4 SHRIMP results

Individual spots on APS minerals and overgrown alunite were analyzed for S-isotopic composition by ion probe, with spot size ~30 μm (Fig. 7, inset). The two samples are from drill hole U80-23 (Fig. 2) at ~870 and 730 m elevation, over the top of the FSE deposit (Aoki and Eldridge, 1994).

Euhedral woodhouseite crystals in U80-23-117' are zoned (Fig. 7a, b), whereas woodhouseite clusters in U80-23-596' (Fig. 7c-e) are strongly corroded and show less

evidence of zoning. The crystals are 250 to >500 μm in size and are overgrown by alunite and irregular crystals of pyrite. Three woodhouseite crystals (Fig. 7) returned $\delta^{34}S$ values of 14 and 16 permil, 21 and 15 permil, and 16 and 15 permil, with no clear variation related to position on the crystals. Overgrowths of alunite plus one crystal of anhydrite returned $\delta^{34}S$ values of 20, 18, 21 and 28 permil (Fig. 7a), 13, 16 and 12 permil (Fig. 7b), 18 permil (Fig. 7d), and 16 (anhydrite) and 15 permil (Fig. 7e), with analyses from 50 to 500 μm away from woodhouseite crystals. There is not any obvious spatial correlation of alunite $\delta^{34}S$ values, which vary from 12 to 28 permil. Alunite is heavier (18, 20, 21, 28 permil) than woodhouseite (14, 16 permil) in one section (Fig. 7a), slightly lighter in another (12, 13 and 16 permil) versus woodhouseite (15, 21 permil), and similar in the deeper sample (18 permil versus 15, 16 permil). Pyrite from U80-23-117', adjacent to the woodhouseite crystal (Fig. 7a), has a $\delta^{34}S$ composition of -4 permil, and two pyrite crystals from U80-23-596' have values of 1 permil, and 2, 1 and -4 permil, the latter >1 mm in size (Fig. 7c).

Three analyses of alunite on spots immediately adjacent to one another (Fig. 7, inset) returned $\delta^{34}S$ values of 20, 18 and 21 permil, and two adjacent spots on pyrite (Fig. 7c) returned values of 2 and 1 permil. This reproducibility (although the repeat analyses were not in the exact same place, with center points separated by ~30-40 μm) is within the reported SHRIMP error of ±2 permil $\delta^{34}S$.

4.5 Sulfate-sulfide fractionation temperatures

The S-isotopic results for sulfate and sulfide minerals separated from the same hand samples or drill core are reported in Appendix Table 1. In cases where the presumption of equilibrium between minerals was questionable, such as where minerals were not in contact (i.e., from adjacent samples), or were from stages interpreted to be different in the same sample, the calculated temperature is listed in brackets.

Stage-1 alunite-pyrite pairs have fractionation temperatures that range from 202 to 224°C, with the four samples coming from footwall and hanging wall structures; two other alunite samples, with cross-cutting enargite used as the sulfide (values in parentheses; Fig.

9) return 200, 221 and 223°C. By contrast, two alunite (and the APS mineral woodhouseite) samples, over the top of the FSE porphyry at 870 and 730 m elevation and analyzed by SHRIMP, record temperatures as high as 398°C and as low as 225°C (with one particularly heavy alunite indicating 166°C, assuming constant $\delta^{34}S$ of pyrite). Four analytical spots on alunite and APS from the deeper sample have a small (3 permil) variation, whereas four pyrite analyses returned a range of 6 permil $\delta^{34}S$ (–4 to 2 permil; 1 permil was used for calculations). Only one pyrite was analyzed in the shallower sample, –4 permil, but data were gathered on 10 sulfate spots (12 to 21 permil, with one result at 28 permil) and six spots on APS minerals (14 to 21 permil). The results indicate that alunite (and to a lesser extent APS minerals) plus pyrite can have large local variations in S-isotopic composition. Another alunite-pyrite sample ~250 m to the NW at 680 m elevation (the deepest alunite analyzed) returned 320 and 362°C, using results from repeat alunite analyses (Appendix Table 1).

The copper (and gold) mineralization related to stage-2 anhydrite and barite is associated with chalcopyrite plus pyrite in FSE and enargite in Lepanto, respectively. Locations below sea level return fractionation temperatures of 329, 352 and 391°C from one sample, with other samples as high as 493°C (but also 320°C from another pair in the same thin section) to 406°C. From sea level to 680 m elevation, six anhydrite-pyrite pairs return temperatures of 250 to 320°C. Within the Lepanto ore body >1 km to the NW, barite-chalcopyrite and barite-enargite pairs indicate 233 and 199°C, respectively.

The sulfate-sulfide (alunite-pyrite) fractionation temperatures, plotted in a SE to NW long section from FSE to Lepanto (Fig. 9), indicate the location of the approximate 300 and 200°C isotherms of the hydrothermal system during early stage-1 alteration. In comparison with later stage-2 sulfate (anhydrite and barite) and sulfide (chalcopyrite, enargite and pyrite) fractionation values, the calculated temperatures suggest that the 300 and 200°C isotherms receded towards the core of the FSE porphyry from stage 1 to stage 2, shifting more than 500 m laterally to the SE within Lepanto and 500 m vertically within FSE (Fig. 9). In addition, the 300 and 200°C isotherms of the hydrothermal system during the main stage of mineralization (stage 2), as indicated by fluid inclusion homogenization

temperatures documented for the Lepanto (Mancano and Campbell, 1995) and FSE (Hedenquist et al., 1998) deposits are shown on Figure 9. Allowing for variation between methods for determination of paleotemperatures (fluid inclusions versus S-isotopic fractionation), the results are consistent with cooling and isotherm recession from stage 1 to stage 2.

5.0 Discussion

Hydrothermal fluid framework from O and H isotopes, and fluid-inclusion data

The FSE porphyry deposit is the center of the hydrothermal system, with early potassic alteration near sea level indicating a high-temperature environment, >500°C (Shinohara and Hedenquist, 1997; Hedenquist et al., 1998). By contrast, the stability of alteration minerals (pyrophyllite, diaspore, dickite, nacrite, kaolinite and alunite) of the contemporaneous advanced argillic lithocap, which formed above ~650 m elevation, indicate temperatures of ~350 to 200°C (Hemley et al., 1980; Watanabe and Hedenquist, 2001; Chang et al., 2011). The hydrothermal biotite and alunite of the potassic and lithocap alteration, respectively, were contemporaneous at ~1.4 Ma (Fig. 9; Arribas et al., 1995a). These stage-1 alteration minerals formed from coupled hypersaline liquid and vapor, respectively; after the vapor separated from the liquid it ascended and condensed to form an acidic solution that leached the rock and created the alunite of the lithocap. The alunite in the lithocap directly over the porphyry has oxygen and hydrogen isotopic compositions expected for end-member magmatic vapor condensed by a 15% meteoric water component (Hedenquist et al., 1998). Further to the NW, alunite compositions show evidence for a progressive dilution of this magmatic vapor condensate by local meteoric water, from 25 to 35% in the center of the Lepanto ore body to as much as a 50% meteoric water component at the furthest sample location, ~4 km NW of the porphyry (Fig. 9). The O and H isotopic compositions of subsequent stage-2 white mica and pyrophyllite of the porphyry deposit, and more distal dickite and nacrite in the lithocap, show evidence for a similar NW-directed flow and meteoric-water dilution (Hedenquist et al., 1998).

As an independent check on the meteoric water component and the degree of

cooling, critical-behavior vapor (>373°C, with an enthalpy of ~2100 kJ/kg) condensed by a 15% meteoric component would produce ~340°C liquid condensate; this mixed with an additional meteoric component during outflow to the NW (to reach a total of 35 and 50% in the center and distal portion of the lithocap, respectively, as indicated from O and H stable isotopic compositions). A mass-enthalpy calculation indicates temperatures of ~260 and ~210°C for the mixtures, respectively, similar to that determined from alunite-pyrite pairs. The diluent used was steam-heated (~100 °C) meteoric water, as indicated from extending the fluid-inclusion temperature-salinity mixing trend to nil salinity (Hedenquist et al., 1998); a 20°C meteoric-water diluent would result in slightly lower temperatures, as would heat loss to the surrounding rock.

Fluid inclusion homogenization data (Appendix Table 1) from stage-2 euhedral quartz veins, associated with white mica alteration (Hedenquist et al., 1998), record 350 and 280°C from the core and the margin of the porphyry deposit, respectively (Fig. 9, ~0 mL elevation). These findings are consistent with data from stage-2 enargite-hosted fluid inclusions (Mancano and Campbell, 1995) in the epithermal deposit, which range from 294°C at 592 m elevation over the FSE deposit to 196 °C at the distal limit of enargite (Fig. 9). The data from these stage-2 minerals are interpreted to indicate that the same white mica-stable liquid was present in both environments (Hedenquist et al., 1998). Cooling from ~350°C in the porphyry to 200°C in the epithermal deposit was caused by meteoric-water dilution (similar to that noted for the stage-1 condensate), as indicated by the decrease from 5 wt% NaCl equivalent salinity at the porphyry level (in quartz veins associated with white mica alteration) to <2 wt% NaCl equivalent (in enargite-hosted inclusions) at the distal limit of the ore body (Fig. 13 in Hedenquist et al., 1998). Cooling as the liquid ascended to ~1000 m elevation during lateral flow, a distance of over ~2 km to the NW, caused enargite deposition within the residual quartz zone of the lithocap (Fig. 9). The shift from intermediate sulfidation-state chalcopyrite stability at ~350 °C in the porphyry (as well as tennantite; Imai, 2000) to high sulfidation-state enargite stability at 300 to 200°C, is characteristic of such deposits worldwide, due to cooling in the buffer-free residual quartz of the silicic lithocap (Einaudi et al., 2003).

S isotopic variation

The existing framework (Hedenquist et al., 1998) indicates cooling with distance from the porphyry center and with time. The evolution in S-isotopic composition of stage-1 and -2 sulfide and sulfate minerals also indicates a consistent pattern, albeit with some complexities. The starting point of this discussion is the total S-isotopic composition of the source intrusions, as indicated by two samples of least-altered Imbanguila diorite (age ~2 Ma; Arribas et al., 1995a). Values of 2.0 permil (Appendix Table 1) are typical of the $\delta^{34}S$ values of igneous rocks and associated ore deposits in arc systems (average of ~2 to 5 permil; Sasaki and Ishihara, 1979, 1980).

Stage 1: The deepest S-bearing stage-1 minerals analyzed are alunite-pyrite pairs from 680 to 870 m elevation, over the top of the FSE porphyry deposit. These pairs indicate equilibrium temperatures of 411 to 320°C, although one particularly heavy $\delta^{34}S$ value of 28 permil (by ion probe) indicates 166°C if in equilibrium with the pyrite used for calculation (1 permil; Appendix Table 1). The stage-1 pyrite from 680 to 870 m elevation, both from conventional analysis and by ion probe, ranges from –4 to 2 permil $\delta^{34}S$ (Appendix Table 1); individual spots within 500 μm of each other in one pyrite crystal vary by this range of 6 permil (Fig. 7c). Thus, the single pyrite value analyzed from one sample at 870 m elevation (U80-23-117'; Appendix Table 1), –4 permil $\delta^{34}S$, may not be the appropriate indicator of the sulfide value to use as a pair for all alunite values from this one thin section, which has a 16 permil $\delta^{34}S$ range (Fig. 7a, b) over a few mm. The ion probe variation within single crystals is greater than expected from the ±2 $\delta^{34}S$ permil error for the ion probe technique, whereas conventional replicate analyses indicate smaller variation, probably due to the larger sample aliquots being homogenized. The wide variation of S-isotopic composition of stage-1 sulfates in the same crystals (16 permil $\delta^{34}S$; Fig. 7) from 680 to 870 m elevation – more than can be accounted for by the observed shifts in pyrite values (6 permil) due to variations in redox conditions – suggests that there were also sharp variations of temperature at this level over the top of the porphyry deposit and associated intrusions. These samples suggest a redox state of ~2:1 H_2S/SO_4.

To the NW in the Lepanto deposit, from 700 to 1030 m elevation, other stage-1 alunite-pyrite pairs returned S-isotopic fractionation temperatures of 224 to 202°C, with no strong temperature zonation along the 2-km lateral extent of the proximal, mineralized half of the lithocap (Fig. 9). This indicates that the high-temperature (~350±50°C) acidic condensate directly over the porphyry deposit cooled to <250°C within an interval of ~400 m of lateral flow to the NW (Fig. 9), indicating a highly permeable hydrologic system to allow mixing with steam-heated meteoric water (see above). The cooling to ~200°C over the ~2 km interval would have caused an increase in reactivity (Hedenquist and Taran, 2013), resulting in leaching of the rock and formation of residual quartz in the thickest portion of the lithocap. The offset of the main lithocap from the underlying location of the porphyry deposit was caused by lateral flow caused by the NW-directed hydraulic gradient at ~1.4 to 1.3 Ma (Hedenquist et al., 1998).

Stage 2 porphyry level: Subsequently, the deep system evolved to stage 2 of phyllic alteration (Hedenquist et al., 1998). Near sea level (±100 m), stage-2 minerals include chalcopyrite (1.6 to 2.6 permil $\delta^{34}S$; avg. 2.1 permil, n=4), pyrite (1.1 to 3.0 permil; avg. 2.5 permil, n=7) and anhydrite (13.2 to 23.4 permil, n=10). This is similar to the range of $\delta^{34}S$ values reported by Imai (2000) for the same minerals at this level, and who also recorded $\delta^{34}S$ values of anhydrite as light as 12.4 permil near sea level in the center of the deposit. There is a relatively large range in anhydrite composition for some individual samples (range up to 7 permil), based on micro-drilling results (13.2 and 21.3, and 16.8 to 20.3 permil $\delta^{34}S$; Appendix Table 1, Bunce, 2015).

The average values of deep chalcopyrite and pyrite samples are similar to the whole-rock $\delta^{34}S$ value of 2.0 permil. This similarity of total $\delta^{34}S$ value to that of the sulfide $\delta^{34}S$ value during stage 2 of the deep porphyry system indicates a relatively reduced parent fluid at depth, i.e., $SO_2<H_2S$, such that temperature fluctuations would be reflected mostly in the sulfate $\delta^{34}S$ value due to the large leverage. Based on the whole-rock $\delta^{34}S$ value and compositions of coexisting sulfide minerals and anhydrite, the H_2S/SO_4 ratio was determined by the lever rule, and may have been ~10:1 during stage-2 copper deposition in the porphyry deposit. The much larger S-isotopic variation of anhydrite (~10 permil)

than coexisting stage-2 sulfides (~2 permil) near sea level must have been caused by temperature fluctuations from such a sulfide-dominant fluid (e.g., local fluid pulses up to ~450+ ^{o}C in a 300-350 ^{o}C system).

The white mica-stable (phyllic) stage-2 quartz has fluid inclusion homogenization values of 350^{o}C at 90 m elevation in the center of the porphyry deposit (E400 section), and 280^{o}C on the western margin at 80 m elevation (Hedenquist et al., 1998; Appendix Table 1). S-isotopic temperatures ($\Delta\ ^{34}S_{sulfate\text{-}sulfide}$; Appendix Table 1) of samples from 0 to 110 m elevation on the western margin (E10 section) are 255 and 281^{o}C, similar to the fluid inclusion values. To the east (E400 to E540 sections), equilibrium temperatures from samples at –30 to –100 m elevation range from 320 to 493^{o}C, and 285^{o}C at 90 m elevation. Compared to the fluid inclusion homogenization value of 350^{o}C at 90 m, the deeper samples report 30^{o}C lower to 145^{o}C higher temperatures from mineral pairs, and 65^{o}C lower for the 90-m elevation pair, which comes from the same sample (U83-34-2121'; Appendix Table 1) as the fluid-inclusion measurement. If these pairs reflect equilibrium conditions, they would indicate pulses of high-temperature magmatic fluid that were not reflected in the fluid-inclusion result. Alternatives would be disequilibrium conditions or possible contamination of the anhydrite by pyrite (the micro-drilling of the FSU samples by Bunce, 2015, was undertaken with care during examination by binocular microscope, to avoid contamination).

Stage 2 lithocap level: Stage-2 anhydrite-pyrite pairs from 430 to 680 m elevation at the top of the FSE deposit returned temperatures of 362 to 242^{o}C, with enargite fluid-inclusion results from 592 m having the highest enargite homogenization value of 294^{o}C (Appendix Table 1). One anhydrite-sulfide pair in the Lepanto vicinity from 680 m indicates a value of 250^{o}C. By contrast, three values from stage-2 barite-sulfide gangue in the Lepanto ore body at the 1030 to 1100 mL, NW of the Tubo shaft, return values of 233 to 199^{o}C, consistent with the lower temperatures from stage-2 enargite-hosted fluid inclusions (241 to 196^{o}C; Fig. 9) in this portion of the lithocap-hosted outflow.

All stage-2 enargite and pyrite (as well as stage-1 pyrite) at the level of the lithocap have negative $\delta^{34}S$ values. The average $\delta^{34}S$ value of 14 stage-2 enargite samples from the

Main Ore Body (including three pyrite and one sphalerite; duplicate analyses averaged) is –4.2 permil (range –9.7 to –1.1 permil), and the average of 14 enargite samples from FW and HW structures (including two pyrite, one luzonite and one chalcopyrite) is –3.1 permil (Appendix Table 1). Seven stage-1 pyrite samples from FW and HW structures average –1.7 permil (–2.9 to –0.5 permil); one stage-1 pyrite from the Main Ore Body, far to the NW, is the lightest at –11.8 permil (Appendix Table 1). The large range in $\delta^{34}S$ values of Lepanto sulfides (Fig. 8), particularly during stage 2 (average –4 and –3 permil in the Main Ore Body and HW plus FW structures, respectively), is consistent with a more oxidized fluid at this shallow level (H_2S/SO_4 ~4), in contrast to that in the deep porphyry deposit during stage 2. Such higher oxidation states are typical of the lower temperature portions of magmatic-hydrothermal systems (Arribas, 1995; Einaudi et al., 2003; Hedenquist and Taran, 2013).

Redox variation: Rocks of nearby Pinatubo volcano, ~200 km to the south, record a range of oxidation conditions during its evolution, culminating in a mafic-driven cataclysmic eruption of dacite in 1991 (Hattori, 1993), with mafic xenoliths hosted by the erupted dacite. The water-rich dacite contained sulfide globules and S^{2-} in the melt (Hattori, 1997), but input of SO_2 from an underlying mafic source may have further oxidized the dacite magma to ~NNO+1.5 to 2 (Scaillet and Evans, 1999). The SO_2 from the mafic melt, after reduction, provided S^{2-} to form sulfide minerals that precipitated metals added by the mafic melt to the overlying dacite magma chamber (de Hoog et al., 2004). This example may be relevant to the FSE system, where Imbanguila diorite also hosts mafic xenoliths (P.N. Dunkley, pers. commun., 2015). Evidence for fluctuations in temperature as well as redox state in the FSE porphyry deposit during stage 1 and 2, ~2:1 to 10:1 H_2S/SO_4 ratio, respectively, may have been associated with pulses of hot SO_2-rich fluid (possibly during stage 1?), linked to periodic injection of mafic melt into more silicic magma chambers.

6. Summary and Conclusions

Previous studies of the FSE porphyry system have established that a magmatic fluid was present during early alteration of stage 1 and mineralization of stage 2, both in the FSE

porphyry Cu-Au deposit and the main portion of the Lepanto lithocap and high-sulfidation Cu-Au deposit (Hedenquist et al., 1998). Stage-1 quartz-alunite-pyrite in the lithocap of the FSE porphyry system, above ~650 m elevation, formed from condensates of magmatic vapor at ~1.4 Ma, at the same time as potassic alteration formed from hypersaline liquid near sea level, with the vapor and hypersaline liquid being coupled in timing (Arribas et al., 1995) and thus origin.

The S-isotopic composition of the stage-1 alunite and pyrite in this study indicates condensate temperatures >300°C (320 to 411°C) directly over the porphyry deposit, where the magmatic vapor was condensed by a small (~15%) component of meteoric water (Hedenquist et al., 1998; Fig. 9). As the acidic condensate flowed down the hydraulic gradient to the NW, forming the lithocap near the basement-dacite unconformity along the Lepanto fault, meteoric-water dilution increased to 25-50%. This dilution caused a temperature decrease, 224 to 202°C for alunite-pyrite pairs, resulting in increased reactivity due to acid dissociation as the temperature decreased (Hedenquist and Taran, 2013), leading to leaching and the formation of residual quartz in the lithocap.

The S-isotopic temperatures ($\Delta^{34}S_{sulfate\text{-}sulfide}$) of stage-2 minerals indicate temperatures as high as 400+°C near sea level in the porphyry deposit, ≥300°C at the base of the lithocap at ~700 m elevation, cooling to <250°C within the main lithocap at ~900 to 1100 m elevations, and as low as ~200°C at the limit of the Lepanto orebody, ~2 km NW of the porphyry (Fig. 9). These results agree with stage-2 fluid-inclusion homogenization temperatures of hydrothermal quartz within FSE (Hedenquist et al., 1998) and enargite from Lepanto (Mancano and Campbell, 1995). The cooling within silicic-altered host rock in the lithocap was largely due to dilution by steam-heated meteoric water, which resulted in the deep chalcopyrite-stable fluid of stage 2 evolving to high sulfidation-state enargite stability and mineral deposition within the residual quartz of the lithocap. The negative $\delta^{34}S$ compositions of enargite and pyrite, compared to the positive values of sulfate minerals, indicates a H_2S/SO_4 ratio of ~4 within the lithocap, similar to that of other high-sulfidation deposits worldwide (~3 to 5; Arribas, 1995).

The variation in temperature, spatially and during change from stage 1 to stage 2 (Fig. 9), indicates an overall cooling trend as the FSE porphyry system evolved. The 300°C isotherm descended ~500 m from a position over the FSE porphyry, from stage-1 potassic to stage-2 phyllic, although the wide range of $\delta^{34}S$ values of stage-1 alunite over the top of the porphyry deposit and stage-2 anhydrite within the porphyry deposit indicates intermittent periods (pulses) of higher temperature fluid. The distal 200°C isotherm shifted at least 500 m, from the NW to the SE along the Lepanto lithocap and toward the porphyry, from stage 1 to 2. The thermal pulses above the porphyry deposit are best recorded by detailed ion probe results. Large fluctuations in the $\delta^{34}S$ values of stage-1 alunite and APS minerals (up to 16 permil), within 0.5 mm in the same sample, as well as in associated pyrite (up to 6 permil), provide evidence for sharp temperature changes – as indicated by the fine compositional and isotopic banding – due to pulses of a relatively oxidized fluid with H_2S/SO_4 ratio of ~2:1. By contrast, the average $\delta^{34}S$ values of stage-2 chalcopyrite near sea level are similar to the whole-rock $\delta^{34}S$ value of the least-altered Imbanguila diorite intrusion (2 permil). If this was the bulk $\delta^{34}S$ composition of the stage-2 fluid responsible for most of the copper sulfide deposition, the fluid was more reduced, ~10:1 H_2S/SO_4, than during stage 1. The wider range in composition of coexisting anhydrite (~10 permil) than copper sulfides (~2 permil) in the porphyry deposit also indicates a relatively reduced fluid during the stage-2 temperature fluctuations, based on leverage consideration.

The results of this study, in conjunction with previous work (Garcia, 1991; Arribas et al., 1995; Mancano and Campbell, 1995; Hedenquist et al., 1998; Claveria, 2001; Chang et al., 2011) on the FSE porphyry system – including the Lepanto and Victoria epithermal deposits – have led to general conclusions relevant to other porphyry systems (Sillitoe, 2010). These include the formation lifetime of many porphyry deposits (Arribas et al., 1995), the relation of the potassic stage to the formation of the lithocap, as well as the high sulfidation-state mineralization of the latter by a subsequent, but still magmatic-dominant fluid, during the phyllic-stage overprint (Arribas et al., 1995; Hedenquist et al., 1998), and

the integral association of the intermediate-sulfidation Victoria veins with the porphyry system (Claveria, 2001; Chang et al., 2011).

The present study used both traditional methods as well as an ion probe to determine the isotopic composition of sulfide and sulfate minerals. Although the traditional methods indicate calculated temperatures that are consistent with other methods (mineralogy, fluid inclusions), sharp zonations in chemical and isotopic composition are present, most likely due to thermal pulses associated with a more reduced fluid. The common occurrence of such pulses can be seen in the ubiquitous occurrence of multiple stages of quartz veins in porphyry deposits (Sillitoe, 2010) that are related to rapid overpressure-permeability waves (Weis et al., 2012). Such episodic events are very short relative to the lifetimes of porphyry systems associated with individual intrusions, on the order of $<10^5$ years ($\sim10^4$ years for the initial potassic stage), as determined by dating results (Arribas et al., 1995; Garwin, 2002; Buret et al., 2016) and consistent with the constraints from modeling (Cathles, 1977; Shinohara and Hedenquist, 1997; Weis, 2015). If the episodic fracture events reach the surface, they may be represented by phreatomagmatic activity, such as the eruption of altered material from active volcanic-hydrothermal systems at White Island, New Zealand, and Ontake, Japan (Hedenquist et al., 1993; Minami et al., 2016).

In order to resolve these magmatic fluid pulses and more clearly deduce the processes associated with porphyry systems and the deposition of metals, the chemical and isotopic composition of these pulses must be examined by combining careful paragenetic studies on well-constrained samples with microbeam analyses of zoned minerals. This includes both compositional and S (this study) as well as O (e.g., Fekete et al., 2016) and H isotopic analyses, integrated with information from fluid inclusion assemblages (e.g., Redmond et al., 2004; Landtwing et al., 2005). Such information from porphyry ore deposits can also be contrasted with the evolution of apparently barren intrusive systems (e.g., Rezeau et al., 2016) to determine regional controls on magmatism related to ore genesis.

Acknowledgements: We dedicate this paper to Akira Sasaki, who taught us the laboratory procedures and use of sulfur isotopes, developed and maintained the sulfur isotope laboratory at the Geological Survey of Japan, and conducted some of the analyses reported here. This work would not have been possible without his contributions.

We thank Stewart Eldridge, ANU, for the SHRIMP analyses, Dan Mancano for collecting some of the samples listed here and help with analysis of S isotopic compositions at the Geological Survey of Japan, Matt Bunce for separation of some of the FSE samples, Zhaoshan Chang for help with this project and for assistance with some figures, as well as Elvira Comsti and Alfonso P. de la Cruz, Jr., both of Philippines Mines and Geosciences Bureau, and Rene Claveria, Ateneo de Manila University, for their help. The elemental analyser analyses were conducted at the G.G. Hatch Stable Isotope Laboratory, University of Ottawa, by Wendy Abdi and Paul Middlestead. We thank Lepanto Consolidated Mining Company for access to the mine, as well as Jose S. Garcia, Jr., for guidance and advice in the field, and Lepanto mine staff plus Gold Fields geologists for their assistance with sampling; P.N Dunkley provided the surface samples of Imbanguila diorite, as well as a copy of his internal mapping report. We acknowledge Bryan Yap, President, Lepanto Consolidated Mining Company, and Frederick Louw, President, Far Southeast Gold Resources, Ltd., for permission to publish. This study was initially supported by a grant from the Society of Resource Geology of Japan (then the Society of Mining Geologists of Japan) to JWH. We thank Peter Dunkley and Keiko Hattori for comments on an earlier version of the manuscript and reviews by Minoru Kusakabe and Cari Deyell that improved its clarity. Prof. Shunso Ishihara provided encouragement to write up this research for publication.

References

Aoki, M., 1991, Mineralogical features and genesis of alunite solid solution in high temperature magmatic-hydrothermal systems: Geological Survey of Japan, Report 277, p. 31– 32.

Aoki, M., and Eldridge, S., 1994, Chemical and isotopic heterogeneity in alunite-group minerals indicates a fluctuating and evolving chemical environment in the Lepanto-Far Southeast porphyry-epithermal system, northern Philippine [abs.]: Resource Geology, v. 44, p. 268.

Arribas, A., Jr., 1995, Characteristics of high-sulfidation epithermal deposits, and their relation to magmatic fluid: Mineralogical Association of Canada Short Course, J.F.H. Thompson, ed., v. 23, p. 419-454.

Arribas, A., Jr, Hedenquist, J.W., Itaya, T., Okada, T., Concepción, R.A. and Garcia J.S., Jr., 1995a, Contemporaneous formation of adjacent porphyry and epithermal Cu-Au deposits over 300 ka in northern Luzon, Philippines: Geology, v. 23, p. 337-340.

Arribas, A., Jr., Cunningham, C.G., Rytuba, J.J., Rye, R.O., Kelly, W.C., Podwysocki, M.H., McKee, E.H., and Tosdal, R.M., 1995b, Geology, geochronology, fluid inclusions, and isotope geochemistry of the Rodalquilar gold-alunite deposit, Spain: Economic Geology, v. 90, p. 795-822.

Berger, B.R., Henley, R.W., Lowers, H.A., and Pribil, M.J., 2014, The Lepanto Cu–Au deposit, Philippines: A fossil hyperacidic volcanic lake complex: Journal of Volcanology and Geothermal Research, v. 271, p. 70-82.

Bunce, M., 2015, Gold deportment and trace-element content of copper sulphides of the Far Southeast porphyry copper-gold deposit, Philippines, B.Sc. thesis, University of Ottawa, 117 p.

Bunce, M., Hedenquist, J.W., Hattori, K., and Jackson, S., 2015, Gold and trace-element content of copper sulfides of the Far Southeast porphyry copper- gold deposit, Philippines [abst.], Geological Association of Canada-Mineralogical Association of Canada, Montreal, 11-14 May.

Buret, Y., von Quadt, A., Heinrich, C., Selby, D., Wälle, M., and Peytcheva, I., 2016, From a long-lived upper-crustal magma chamber to rapid porphyry copper emplacement: Reading the geochemistry of zircon crystals at Bajo de la Alumbrera (NW Argentina), Earth and Planetary Science Letters, v. 450, p. 120-131.

Cathles, L.M., 1977, An analysis of the cooling of intrusives by ground-water convection which includes boiling, Economic Geology, v. 72, p. 804-826.

Chang, Z., Hedenquist, J.W., White, N.C., Cooke, D.R., Roach, M., Deyell, C.L., Garcia, J.S., Jr., Gemmell, J.B., McKnight, S. and Cuison, A.L., 2011, Exploration tools for linked porphyry and epithermal deposits: Example from the Mankayan intrusion-centered Cu-Au district, Luzon, Philippines: Economic Geology, v. 106, p. 1365-1398.

Claveria, R.J.R., 2001, Mineral paragenesis of the Lepanto copper and gold and the Victoria gold deposits, Mankayan mineral district, Philippines: Resource Geology, v. 51, p. 97–106.

Claveria, R.J.R. and Hedenquist, J.W., 1994, Paragenesis Au and related minerals in the Lepanto Cu-Au deposit [abs]: Resource Geology, v. 44, p. 267

Concepción, R.A., and Cinco, J.C., Jr., 1989, Geology of the Lepanto-Far Southeast gold-rich copper deposit [abs.], International Geological Congress, Washington, D.C., Proceedings, v. 1, p. 319-320, and preprint, 46 p.

De Hoog, J.C.M., Hattori, K.H. and Hoblitt, R.P., 2004, Oxidized, sulfur-rich mafic magma at Mount Pinatubo, Philippines, Contributions to Mineralogy and Petrology, v.146, p. 750-761.

Deyell, C.L., Rye, R.O., Landis, G.P., and Bissig, T., 2005, Alunite in an evolving magmatic-hydrothermal system: The Tambo high-sulfidation deposit, El Indio district, Chile: Chemical Geology, v. 215, p. 185-218.

Deyell, C.L., Leonardson, R., Rye, R.O., Thompson, J.F.H., Bissig, T., and Cooke, D.R., 2005, Alunite in the Pascua-Lama high-sulfidation deposit: Constraints on alteration and ore deposition using stable isotope geochemistry: Economic Geology, v. 100, p. 131-148.

Dunkley, P.N., 2015, The geology of the Mankayan district, Benguet Province, Luzon, Philippines: Far Southeast Gold Resources Inc., internal report, 66 p.

Einaudi, M.T., Hedenquist, J.W. and Inan, E.E., 2003, Sulfidation state of fluids in active and extinct hydrothermal systems: Society of Economic Geologists and Geochemical Society Special Publication 10, p. 285-313.

Fekete S., Weis P., Driesner T., Bouvier A.-S., Baumgartner L.P., Heinrich C.A., 2016, Contrasting hydrological processes of meteoric water incursion during magmatic–hydrothermal ore deposition: An oxygen isotope study by ion microprobe, Earth and Planetary Science Letters, v. 451, p. 263-271, doi.:10.1016/j.epsl.2016.07.009

Gaibor, A., Dunkley, P., Wehrle, A., Lesage, G., Boer, D. Den, and Froilan, C., 2013, The discovery and understanding of the Far Southeast copper-gold porphyry, Luzon, Philippines: Proceedings, New Gen Gold conference, Pay Dirt Media, Perth, p. 233-247.

Garcia, J.S., Jr., 1991, Geology and mineralization characteristics of the Mankayan mineral district, Benguet, Philippines: Geological Survey of Japan Report 277, p. 21-30.

Garwin, S., 2002, Ore geology setting of intrusion-related hydrothermal systems near Batu Hijau porphyry copper-gold deposit, Sumbawa, Indonesia, in Goldfarb, R.J., and Nielsen, R.L., eds., Integrated method for discovery: Global exploration in the twenty-first century, Society of Economic Geologists Special Publication 9, p. 333-366.

Gonzalez, A.G., 1956, Geology of the Lepanto copper mine, Mankayan, Mountain Province: Philippines Bureau of Mines Special Projects Series 16, p. 17-50.

Gonzalez, A.G., 1959, Geology and genesis of the Lepanto copper deposit, Mankayan, Mountain Province, Philippines, Unpublished Ph.D. dissertation, Stanford University, 102 p.

Hattori, K., 1993, High-sulfur magma, a product of fluid discharge from underlying mafic magma: Evidence from Mount Pinatubo, Philippines: Geology, v. 21, p. 1083-1086.

Hattori, K., 1997, Occurrence of sulfide and sulfate in the 1991 Pinatubo eruption products and their origin, *in* Newhall, C.G. and Punongbayan, R.S., eds., Fire and mud: Eruptions and lahars of Mount Pinatubo, Philippines: University of Washington Press, Seattle, p. 807-824.

Hedenquist, J.W., Arribas, A., Jr. and Reynolds, T.J., 1998, Evolution of an intrusion-centered hydrothermal system: Far Southeast-Lepanto porphyry and epithermal Cu-Au deposits, Philippines: Economic Geology, v. 93, p. 373-404.

Hedenquist, J.W. and Taran, Y.A., 2013, Modeling the formation of advanced argillic lithocaps: volcanic vapor condensation above porphyry intrusions: Economic Geology, v. 108, p. 1523-1540.

Hemley, J.J., Hostetler, P.B., Gude, A.J. and Mountjoy, W.T., 1969, Some stability relations of alunite: Economic Geology, v. 64, p. 599-612.

Hemley, J.J., Montoya, J.W., Marinenko, J.W. and Luce, R.W., 1980, Equilibria in the system Al_2O_3-SiO_2-H_2O and some general implications for alteration-mineralization processes: Economic Geology, v. 75, p. 210-228.

Landtwing, M.R., Pettke, T., Halter, W.E., Heinrich, C.A., Redmond, P.B., Einaudi, M.T., Kunze, K., 2005, Copper deposition during quartz dissolution by cooling magmatic–hydrothermal fluids: The Bingham porphyry, Earth and Planetary Science Letters, v. 235, p. 229-243.

Li, G., Peacor, D.R., Essene, E.J., Brosnahan, D.R., and Beane, R.E., Walthierite, 1992, $Ba_{0.5}\square_{0.5}Al_3(SO_4)_2(OH)_6$, and huangite, $Ca_{0.5}\square_{0.5}Al_3(SO_4)_2(OH)_6$, two new minerals of the alunite group from the Coquimbo region, Chile: American Mineralogist, v. 77, p. 1275-1284.

Imai, A., 2000, Mineral paragenesis, fluid inclusions and sulfur isotope systematics of the Lepanto Far Southeast porphyry Cu-Au deposit, Mankayan, Philippines: Resource Geology, v. 50, p. 151-168.

Mancano, D.P., and Campbell, A.R., 1995, Microthermometry of enargite-hosted fluid inclusions from the Lepanto, Philippines, high-sulfidation Cu-Au deposit: Geochimica et Cosmochimica Acta, v. 59, p. 3909-3916.

Meyer, C. and Hemley, J. J., 1967, Wall-rock alteration, *in* Barnes, H. L., ed., Geochemistry of hydrothermal ore deposits: New York, Holt, Rinehart, and Winston, p. 166-235.

Minami, Y., Imura, T., Hayashi, S., Ohba, T., 2016, Mineralogical study on volcanic ash of the eruption on September 27, 2014 at Ontake volcano, central Japan: correlation with porphyry copper systems, Earth, Planets and Space, v. 68:67 DOI 10.1186/s40623-016-0440-2

Ransome, F.L., 1907, The association of alunite with gold in the Goldfield district, Nevada: Economic Geology, v. 2, p. 667-692.

Redmond, P.B., Einaudi, M.T., Inan, E.E., Landtwing, M.R., Heinrich, C.A., 2004, Copper ore formation by fluid cooling in porphyry copper deposits: new insights from cathodoluminescence petrography combined with fluid inclusion microthermometry, Geology, v. 32, p. 217–220.

Rezeau, H., Moritz, R., Wotzlaw, J.-F., Tayan, R., Melkonyan, R., Ulianov, A., Selby, D., d'Abzac, F.-X., Stern, R.A., 2016, Temporal and genetic link between incremental pluton assembly and pulsed porphyry Cu-Mo formation in accretionary orogens, Geology, v. 44, p. 627-630, doi:10.1130/G38088.1

Rye, R.O., Bethke, P.M., and Wasserman, M.D., 1992, The stable isotope geochemistry of acid-sulfate alteration: Economic Geology, v. 87, p. 225–262.

Sasaki, A., Arikawa, Y., and Folinsbee, R.E., 1979, Kiba reagent method of sulfur extraction applied to isotope work: Geological Survey of Japan Bulletin, v. 30, p. 241-245.

Sasaki, A. and Ishihara, S., 1979, Sulfur isotopic composition of the magnetite-series and ilmenite-series granitoids in Japan: Contributions to Mineralogy and Petrology, v. 68, p. 107-115.

Sasaki, A. and Ishihara, S., 1980, Sulfur isotopic characteristics of granitoids and related mineral deposits in Japan: Proceedings, 5th IAGOD Quadrennial Symposium, Utah, Scheweizerbart'sche Verlagbuchhandlung, p. 325-335.

Scaillet, B. and Evans, B.W., 1999, The 15 June 1991 eruption of Mount Pinatubo. I. Phase equilibria and pre-eruption P–T–fO_2–fH_2O conditions of the dacite magma: Journal of Petrology, v. 40, p. 381–411.

Seal, R.R., II, 2006, Sulfur isotope geochemistry of sulfide minerals, in Mineralogical Society of America, Reviews in Mineralogy and Geochemistry, Ch. 12, v. 61, p. 633-677.

Shinohara, H., and Hedenquist, J.W., 1997, Constraints on magma degassing beneath the Far Southeast porphyry Cu-Au deposit, Philippines: Journal of Petrology, v. 38, p. 1741-1752.

Sillitoe, R.H., 1983, Enargite-bearing massive sulfide deposits high in porphyry copper systems: Economic Geology, v. 78, p. 348-352.

Sillitoe, R.H., 1995, Exploration of porphyry copper lithocaps, *in* Mauk, J.L., and St. George, J.D., eds., Pacific Rim Congress 1995, Auckland, Proceedings: Parkville, Victoria, Australasian Institute of Mining and Metallurgy 9/95, p. 527-532.

Sillitoe, R.H., 1999, Styles of high-sulphidation gold, silver and copper mineralization in the porphyry and epithermal environments, *in* Weber, G., ed., Pacrim '99 Congress, Bali, Indonesia, 1999, Proceedings: Parkville, Victoria, Australasian Institute of Mining and Metallurgy, p. 29-44.

Sillitoe, R.H., 2010, Porphyry copper systems: Economic Geology, v. 105, p. 3-41.

Sillitoe, R.H., and Angeles, C.A., Jr., 1985, Geological characteristics and evolution of a gold-rich porphyry copper deposit at Guinaoang, Luzon, Philippines, *in* Asian Mining '85, Manila, Philippines, February 11-14, Institute of Mining and Metallurgy, London, p. 15-26.

Steven, T.A. and Ratté, J.C., 1960, Geology of ore deposits of the Summitville district, San Juan Mountains, Colorado: U.S. Geological Survey Professional Paper 343, 70 p.

Stoffregen, R.E., and Alpers, C.N., 1987, Woodhouseite and svanbergite in hydrothermal ore deposits: products of apatite destruction during advanced argillic alteration: Canadian Mineralogists, v. 25, p. 201-211.

Tejada, M.L.G., 1989, Characteristics of paragenesis of luzonite in the Lepanto copper-gold deposit, Mankayan, Benguet, Philippines: Unpublished M.Sc. thesis, National Institute of Geological Sciences, University of the Philippines, 89 p.

Urashima, Y., Saito, M., and Sato, E., 1981, The Iwato gold ore deposits, Kagoshima Prefecture, Japan: Society of Mining Geologists of Japan Special Issue 10, p. 1-14 (in Japanese with English abst.).

Watanabe, Y. and Hedenquist, J.W., 2001, Mineralogic and stable isotope zonation at surface over the El Salvador porphyry copper deposit, Chile: Economic Geology, v. 96, p. 1775-1798.

Weis, P., Driesner, T., Heinrich, C.A., 2012, Porphyry-copper ore shells form at stable pressure-temperature fronts within dynamic fluid plumes, Science, v. 338, p. 1613-1616.

Weis, P., 2015, The dynamic interplay between saline fluid flow and rock permeability in magmatic-hydrothermal systems, Geofluids, v. 15, p. 350-371, doi: 10.1111/gfl.12100

Figure captions

Fig. 1. Map of the Mankayan mineral district showing the distribution of volcanic units, the surficial extent of hydrothermal alteration zones (silicic [residual quartz] ± quartz-alunite ± pyrite, dickite ± kaolinite ± pyrite, illite and/or smectite ± pyrite, and white mica + pyrite ± stockwork veins), based on mapping by Garcia (1991) and Chang et al. (2011), and the surface projection of the Lepanto and FSE ore zones. Stratigraphic units and alteration are revealed by river erosion in the western third of the district (streams shown with blue lines). Diagram modified from Chang et al. (2011). Line of cross section in Figures 2 and 9 indicated by wide gray bar.

Fig. 2. Simplified WNW-ESE longitudinal section through the Lepanto and FSE deposits, approximately in the plane of the Lepanto fault (Fig. 1). The approximate extent of enargite-Au ore in the Lepanto deposit, which is largely hosted by silicic alteration with a halo of quartz-alunite, is shown (Garcia, 1991). This lithocap alteration follows the contact of the Imbanguila Fm with the basement volcaniclastic rocks. The location of the samples from the Lepanto underground mine studied (Appendix Table 1) are plotted on the 680 to 1150 m elevation levels, with other samples from the FSE ore body collected from underground drill holes. The S-isotopic values of stage-1 and -2 sulfide and sulfate minerals are also plotted. Section modified from Concepción and Cinco (1989) and Garcia (1991). The gold and copper grade shells of the FSE deposit are from Gaibor et al. (2013), projected on to the section. Sample points with sample identifier but no sulfur isotope results are shown to provide spatial reference locations (see Fig. 9 for associated analytical data, such as enargite-hosted fluid inclusion homogenization temperatures).

Fig. 3. a) Hydrothermal breccia cemented by stage-1 alunite (al, 1.35±0.10 Ma), then cut by stage-2 sulfide veinlets of pyrite and enargite (s, 930218-3, 680 m level; Appendix Table 1). Width of view 5 cm. b) Hydraulic-fractured breccia of stage-1 residual quartz (rq) cemented by stage-2 enargite, luzonite and minor pyrite (s, Spanish workings; Fig. 1). Scale

divisions in cm (photograph by Z. Chang).

Fig. 4. a-c) Photomicrographs of FSE mineral relationships (a-c), from near sea level to -400 m elevation (transmitted and reflected light, partly crossed polars; FSU 10 and 37 sample positions not plotted on Fig. 2). a) FSU 66-897.5 m. Early pyrite replaced by chalcopyrite and bornite; copper sulfides are intergrown with anhydrite and quartz. b) FSU 10-1393.2 m. Early corroded pyrite replaced by chalcopyrite and bornite; the copper sulfides are intergrown with flakes of white mica. c) FSU 37-855.8 m. Bornite-chalcopyrite-anhydrite vein with white mica halo in a quartz groundmass; bornite replaced by chalcocite and digenite. d) Lepanto sample, stage-2 luzonite plus pyrite cut by veinlet of tennantite with blebs of tetrahedrite plus gold, calaverite and petzite (Claveria and Hedenquist, 1994). Abbreviations: pyrite, py; chalcopyrite, cp; bornite, bn; chalcocite, cc; digenite, dg; luzonite, lz; tennantite, tn; tetrahedrite, td; gold, Au; calaverite, ca; petzite, pe, quartz, qz; anhydrite, an; white mica, wm.

Fig. 5. a) Photomicrograph of Pb-rich woodhouseite (high-relief core) with an elongate overgrowth of banded alunite and natroalunite, plus inclusions of diaspore (small high-relief grains in alunite), set in a matrix of quartz. Sample U80-23-66', 890 m elev., cross-polarized light; width = 0.3 mm. b-d) Backscattered electron images (BEI) of alunite and APS minerals (brighter areas indicate heavier molecular weights of minerals). Samples are located progressively further from the vicinity of the FSE deposit. b) Pb- and P-rich cores of APS minerals with darker epitaxial overgrowths of alunite and natroalunite (alunite is brighter than natroalunite), located above the FSE deposit, U80-23-66', 890 m elev.; width = 0.2 mm. c) P- and Sr-rich cores of APS minerals (svanbergite) that have been strongly corroded and replaced by alunite and Na-alunite; Lepanto 1100 m level, 115M, 970 crosscut south; width = 0.1 mm. d) Weakly zoned alunite and Na-alunite with no evidence for heavy-element cores of APS minerals; northwest end of Lepanto runway, at surface (sample 891106-01), ~1100 m elev.; width = 0.7 mm. Electron probe microanalyzer (EPMA) was Shimadzu model 1500, with 15 kv accelerating voltage, 0.1 nA for BEI.

Fig. 6. Trace-element distribution in two euhedral crystals of Pb- and P-rich APS minerals, overgrown by banded alunite and Na-alunite. Sample U80-23-66' (Fig. 5a, b); width of each image = 0.1 mm. a) Backscattered electron image. b) to i) Secondary X-ray maps of S, P, K, Na, Ca, Sr, Ba, and Pb, respectively. EPMA conditions were 15 kv accelerating voltage and 28 nA for X-ray images; scan time was 1.5 to 7 minutes, with longer periods for Pb, Ba and Sr.

Fig. 7. Backscattered electron images of samples analyzed for S-isotopic composition (values of $\delta^{34}S$) by SHRIMP, including woodhouseite (wh), alunite (al), anhydrite (an) and pyrite (py). Ablation pits are ~30 um diameter (inset). a-b) U80-23-117' and c-d) U80-23-596'. Inset (white box) shows location of adjacent ablation pits.

Fig. 8. Ranges of $\delta^{34}S$ values for sulfide and sulfate minerals of stages 1 and 2, both Far Southeast and lithocap-hosted Lepanto deposits. Deep alunite and pyrite samples of stage 1 that lie directly over FSE (680 to 900 m elevation) are noted with an *; other stage-1 Lepanto samples are offset from the FSE deposit, from 680 to 1100 m elevation. Stage-2 samples from FSE were collected from –160 to 530 m elevation, whereas stage-2 lithocap-hosted samples are from 680 to 1100 m elevation (Fig. 2). Appendix Table 1 includes two least-altered whole-rock samples of Imbanguila diorite, collected at the surface by P.N. Dunkley (both with whole-rock values of 2.0 permil $\delta^{34}S$, analyzed at the University of Ottawa).

Fig. 9. Longitudinal section (WNW-ESE) through the Lepanto and FSE deposits. Temperature calculated for coexisting sulfate and sulfide mineral pairs (values in parentheses for sulfide in veins cutting sulfate minerals; Appendix Table 1), as well as fluid inclusion (fi) homogenization values for FSE (Hedenquist et al., 1998) and Lepanto (Hedenquist, unpublished) quartz, plus Lepanto enargite (Mancano and Campbell, 1995). K-Ar ages (Arribas et al., 1995a) are listed with ±2 σ errors for stage-1 biotite (b) of

potassic alteration in the porphyry deposit, and stage-1 alunite within the lithocap; 10 K-Ar dates of stage-2 white mica (illite) samples, all from the porphyry deposit (250 to –130 m elevation; sample locations and dates not shown), range from 1.37 to 1.22 Ma (Arribas et al., 1995). Proportion of meteoric water diluent (%) mixed with the condensed magmatic vapor, as determined from the O and H isotopic compositions of stage-1 alunite samples, is also shown (Hedenquist et al., 1998). The approximate positions of stage-1 and stage-2 isotherms for 300 and 200°C are shown; the deep stage-2 isotherm for 300°C, calculated from $\Delta\ ^{34}S_{sulfate\text{-}sulfide}$ values, is dashed, as results are locally >300°C.

Appendix Table 1: Sulfide and sulfate sample data from the Far Southeast and Lepanto deposits. Included are sample location, elevation, mineral stage, mineralogy, and S-isotopic composition, with calculated S-isotopic fractionation temperature (Seal, 2006), fluid inclusion homogenization temperature (Mancano and Campbell, 1995; Hedenquist et al., 1998) and K-Ar age of alunite (Arribas et al., 1995). Also included are whole-rock total sulfur contents and S-isotopic composition for two least-altered samples of Imbanguila diorite. Samples in which minerals were not coexisting (i.e., stage-2 pyrite cutting stage-1 alunite, or minerals from two adjacent samples) have calculated temperatures listed in [ ].

Appendix Table 1: Sample locations, S-isotopic data and temperatures calculated from mineral pairs, plus fluid-inclusion homogenization values and K-Ar dates										
Sample	Location	Elev.	Sulfides ‰			Sulfates ‰		T °C	T_h °C	age Ma
		m	pyrite stage 1	chalcopyrite-enargite stage 2 (other sulfides)	pyrite stage 2	alunite stage 1	anhydrite-barite stage 2	sulfate-sulfide	enargite, quartz	
Lepanto				*enargite*						
891106-1	surface, end of runway	1090	oxidized			22.1, 23.5			190 qz	1.46±0.06
891106-5	portal, 50 F MOB	1150	-11.8							
891107-19	90 M FW	1100	-0.6							
891107-21	100 L FW	1100		(-8.9,-4.9 lz;-4.3,-4.0 cp)			21.9 ba	233 ba-cp	228 qz	
891107-24	100 L FW	1100	-2.9							
891107-29	115 L FW	1100	-0.5							
930219-1	135 N O2 FW	1100		-3.8						
930219-3	135 N1 FW	1100							241	
891107-11	35 K HW	1070					20.8 ba			
891107-12	35 K HW	1070				23.8				
891107-13	35 K HW	1070				27.0, 17.2				
891107-14	35 K HW	1070				13.4				
U90-4-53m	55 I FW	1070					22.9 ba			
930208-4	50 J4 MOB	1070		-9.5, -9.9					207	
930206-4	10 C3 NOA	1030							196	
891107-1	45 H HW	1030		-4.4						
891107-4	45 H HW	1030				20.8		221		
930403-1	50 M5 MOB	1030		-4.8			23.0 ba	199 ba-en	232	
930209-1	50 J4 MOB	1030		-1.6						
930205-2	70 N3 MOB	1030		-7.2						
930403-2	95 T MOB	1030		-6.8					219	
930402-1	120 S FW	1030							237	
930315-1	PAN 8W	1030		-2.4						
930218-2	20 C MOB	1000							214	
U91-24-275m	35 R HW	1000		-3.1		22.3		[221]		1.44±0.10
930306-3	50 PQ2 HW	1000							231	
U89-34-630'	155 BZ FW	1000	-1.8, -2.9			23.4		218		1.56±0.29
930311-2	45 PO4 HW	950		-1.0, -1.8						
930209-2	45 P4 HW	950							225	
900517-1	103 FZ XC	950				23.7				1.39±0.06

891108-2	105 X MOB	950		-4.5						
930306-2	125 EZ MOB	950							254	
891108-8	130 IZ HW	950		-4.8						
891108-14	155 KZ FW	950		-2.1,-4.8	-3					
930202-2	165 IZ FW	950		-2.6	-0.8				267	
U89-24-137'	145 EZ FW	900		-1.3						
U89-24-559'	160 EZ FW	900	-2.9			24.4		202		1.44±0.08
930213-2 U89-24	185 EZ FW	900		-1.4					245	
891108-23	90 V MOB	842		(-2.6, -3.9 sl)						
891108-25	90 V MOB	842		-2.6	-2.4					
930325-4	135 EZ XCS, MOB	850							252	
930219-2	125 BZ1 MOB 35 blk	700		-7.4	-5.1				223	
U91-42-15.6m	145 JZ FW	700	-0.5			24.6	23.9	224 [231]		1.17±0.16
930212-1	140 GZ MOB	700							259	
930319-1	140 GZ MOB	680		-1			21.7	250		
930218-3	125 FZ O1 vein	680		-1.7	-1.1	25.0, 23.5		[200, 223]		1.35±0.10
FSE				*chalcopyrite*						
930126-1	E 510 140 VZ DW	900		(-4.1 cv vein)			27.3	[183]		
U80-23-29'	E815	890				20.7				1.34±0.20
U80-23-117' (ion probe)	E815	870	-4			20, 18, 21, 28 (16, 14 wood); 13, 16, 12 (21, 15wood)		166-353		
U80-23-596' (ion probe)	E815	730	2, 1, 1, -4			18 (15, 16wood); 15	16	333-398		
891110-4	E 400	700	1.0, 0.0			13		411		
891110-5	E 400	700				8.9				
U85-37-77'	E 475	680	-1.9, -4.0			13.6, 15.8		362, 320		
U85-37-64'	E 475	680					16.9			
U85-21 140 RZ3	E 325	592							294	
UFF92-2-167m		530			2.3		20.1	320		
UFF93-5-274m	E400	430			1.0		24.4	242		

U83-31-1450'	E 400	260					18.8			
U83-14a-1908'	E 440	120			3.4					
U86-6-1944'	E10	110			1.1		23.4	255		
U83-34b-2121	E400	90			1.5		21.5	285	350 qz	
U86-6-2045'	E10	80							280 qz	
U88-5-2291'	E10	0			1.7		22.0	281		
U83-24-2623'	E540	-100			2.6		16.3	406		
FSU58W1-995.2m		-30		2.1, 2.2 cp	2.3		13.2, 21.3	493, 320		
FSU58W1-999.3m		-30			2.3		14.2	458		
FSU10-962.7m		-90			1.5, 3.0, 2.0		17.6, 20.3, 16.8	352, 329, 391		
FSU76-878	off section	250		2.0 cp						
FSU78-900.9		100		2.6 cp						
FSU3-926.5		60		1.6 cp						
FSU66-897.5		10			3.0, 2.4					
FSU58W1-1124		-160			2.7					
Whole rock	Unit		S ‰	Content, %						
PNDLP 1671	Imbanguila diorite	surface	2.0	0.03						
PNDLP 1712	Imbanguila diorite	surface	2.0	0.05						

Samples listed based on elevation (high to low), then from NW (distal) to SE (proximal) for Lepanto; those beginning in 93xxxx from Mancano (1995). Most samples analyzed at the Geological Survey of Japan, except for SHRIMP at ANU. FSU and PNDLP samples courtesy of Far Southeast Gold Resources, Ltd.; FSU samples (Bunce, 2015) were prepared by micro-drilling; they plus PNDLP whole rocks processed by flow-through analyzer, University of Ottawa. The range of S isotopic values reported by Imai (2000) and Berger et al. (2014) on samples provided by the authors are similar to those listed here. Enargite Th values from Mancano and Campbell (1995); quartz Th values from Hedenquist et al. (1998) and Hedenquist, unpublished; alunite dates from Arribas et al. (1995).

Sulfate-pyrite: $6.063*106/[\ln \alpha_{sulfate\text{-}py}-0.56] = T2$ (K), sulfate-chalcopyrite: $6.513*106/[\ln \alpha_{sulfate\text{-}cp}-0.56] = T2$ (K), sulfate-covellite (CuS): $6.423*106/[\ln \alpha_{sulfate\text{-}cv}-0.56] = T2$ (K) (Seal, 2006). Where temperature calculated for stage-1 alunite without pyrite using stage-2 sulfide, value listed in [brackets]. Conventional and flow-through sulfur analyses have an error of ±0.2 ‰ ; SHRIMP error is ±2 ‰

MOB, Main Ore Body (along Lepanto fault); FW and HW, footwall and hanging wall; cp, chalcopyrite; cv, covellite; lz, luzonite; sl, sphalerite; al, alunite; wood, woodhouseite; an, anhydrite; ba, barite; quartz, qz

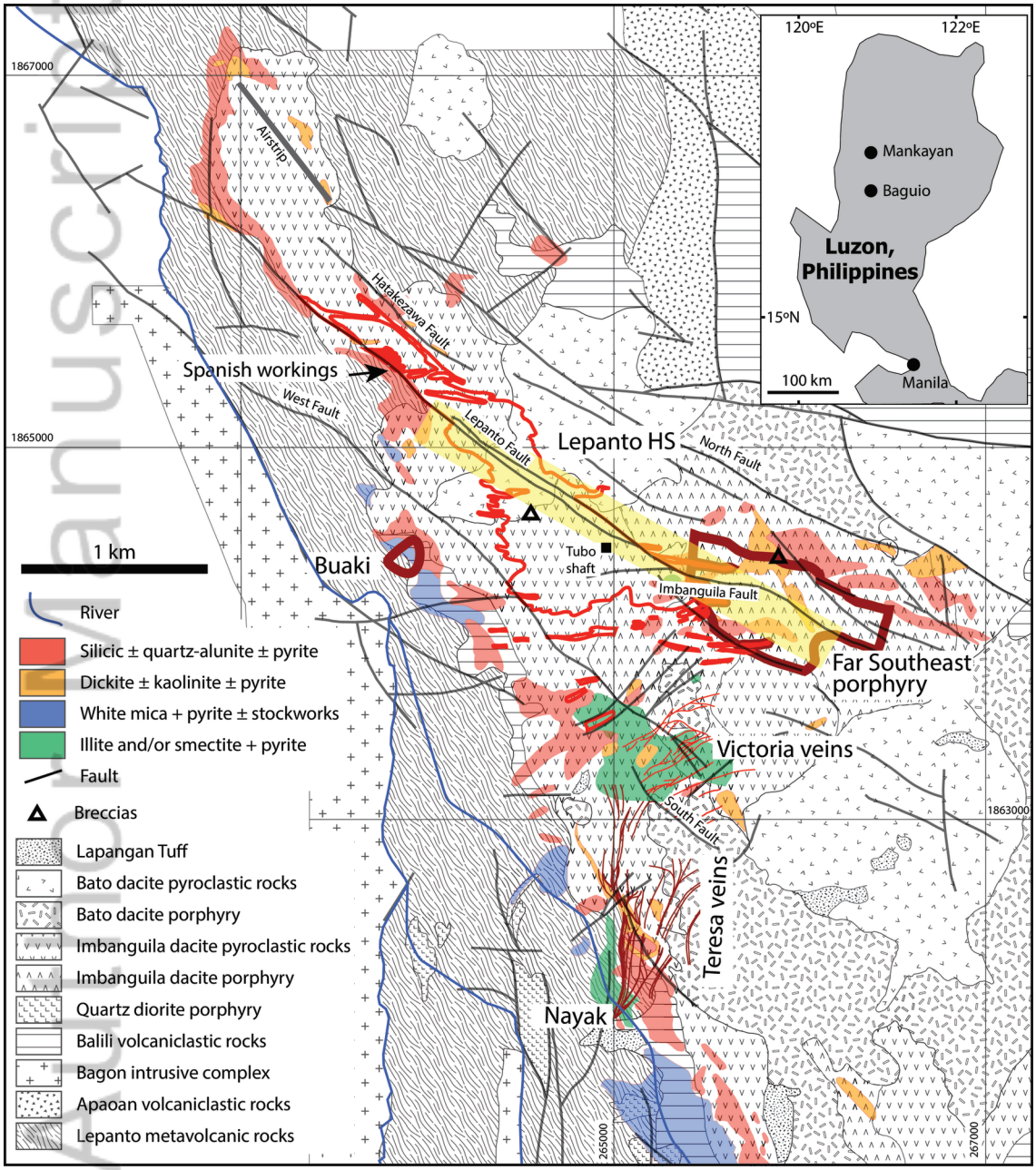

rge_12127_f1.eps

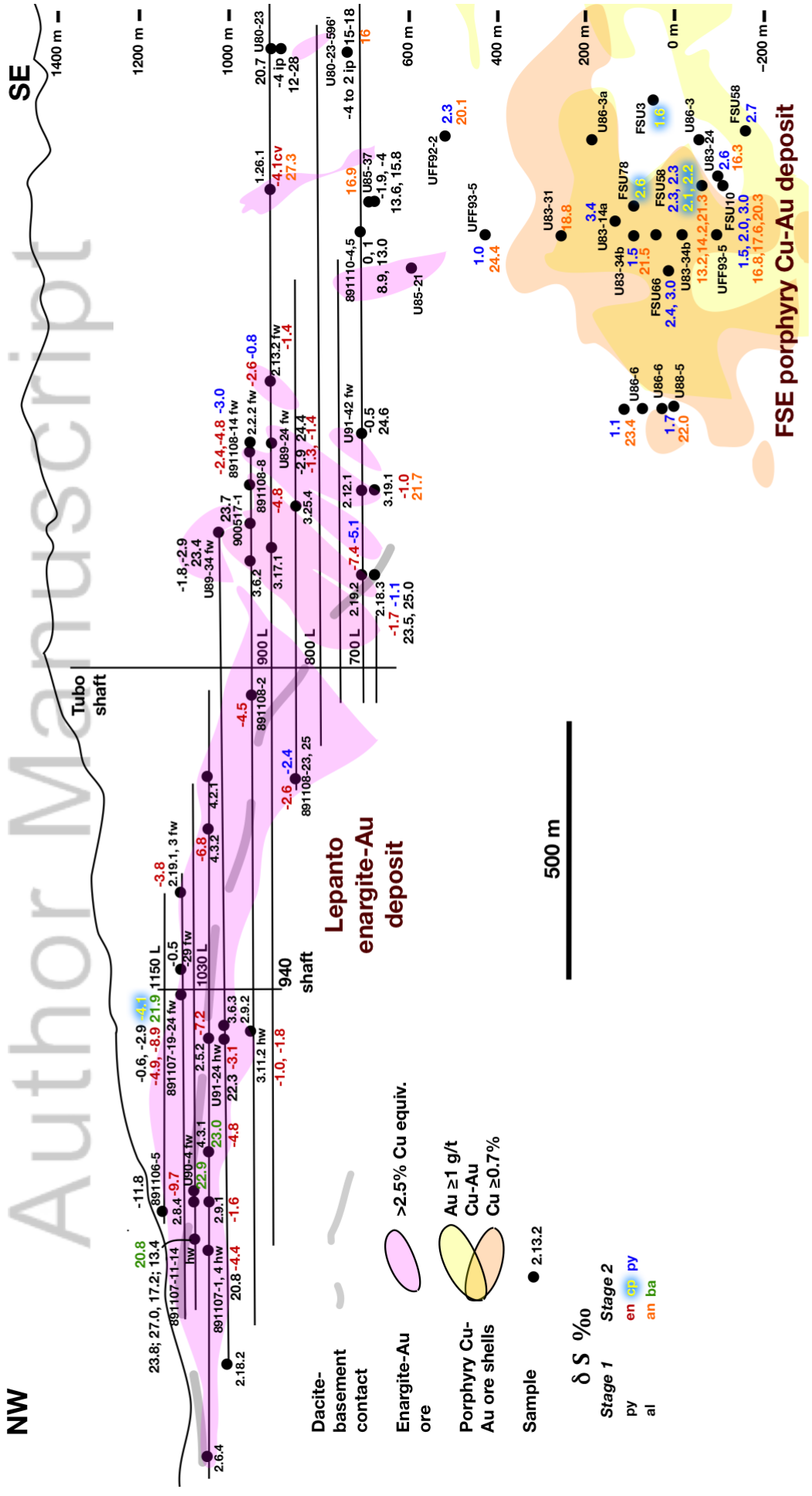

RGE_12127_F2.tiff

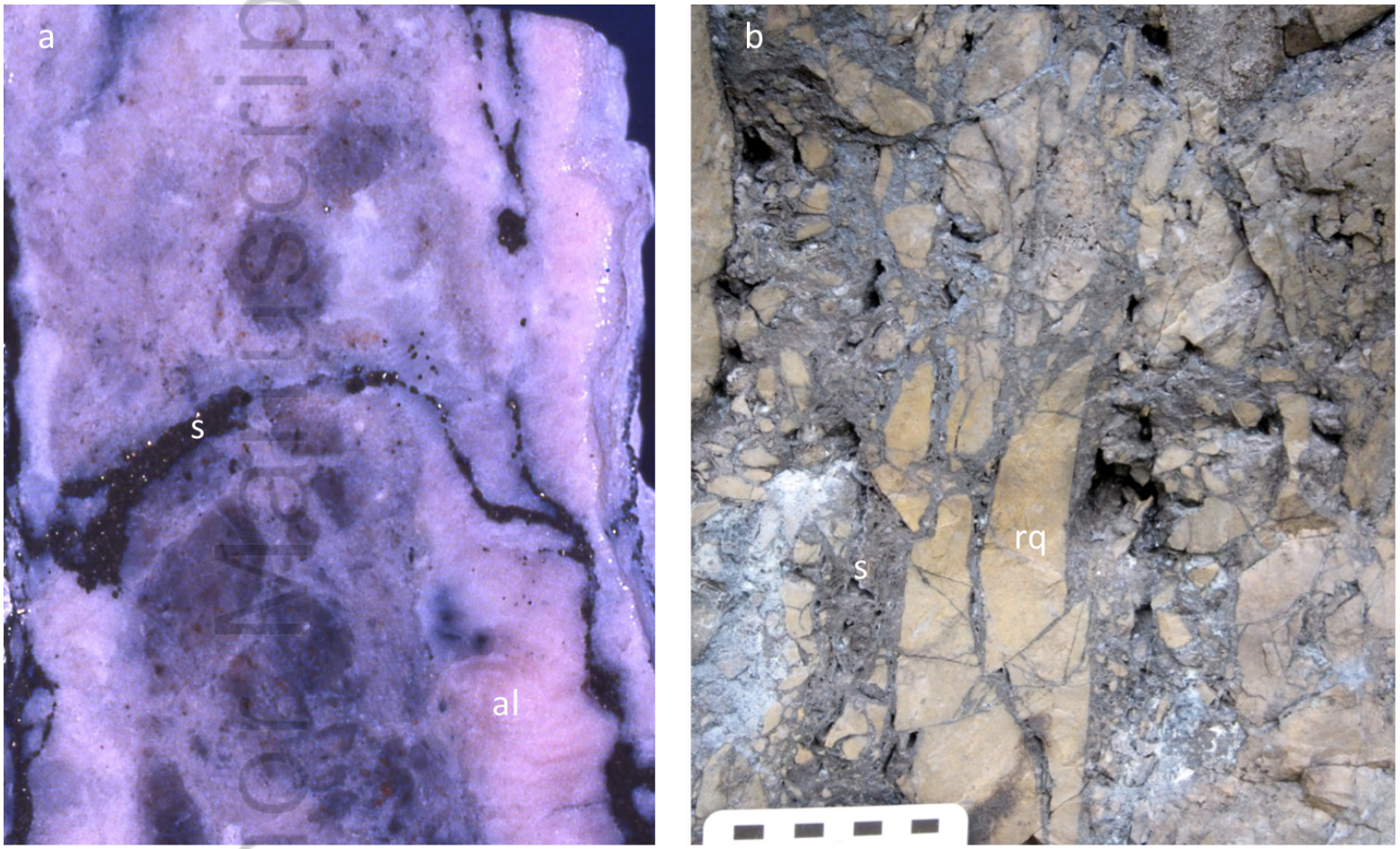

Fig. 3

RGE_12127_F3.tiff

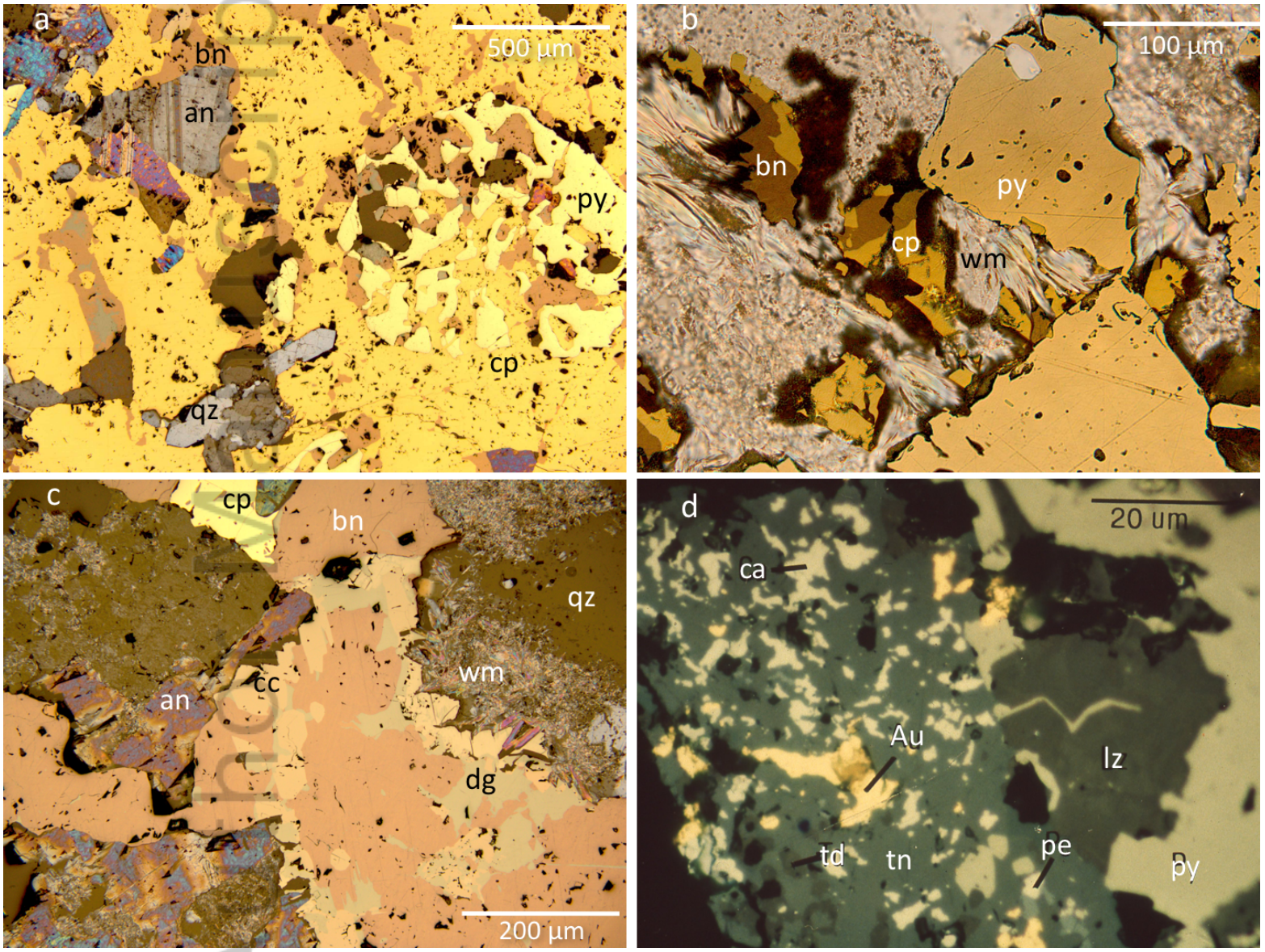

RGE_12127_F4.tiff

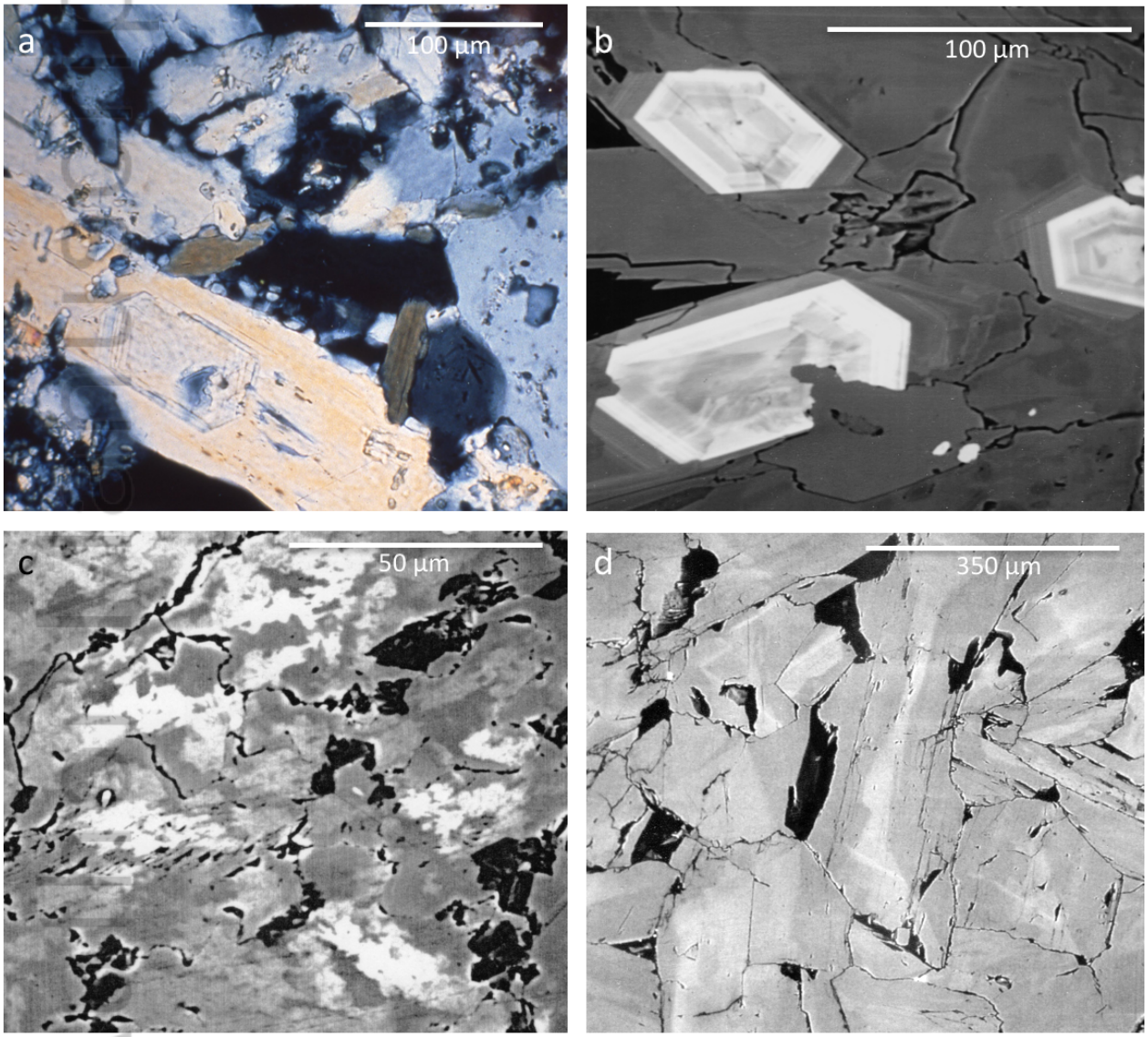

Fig. 5

RGE_12127_F5.tiff

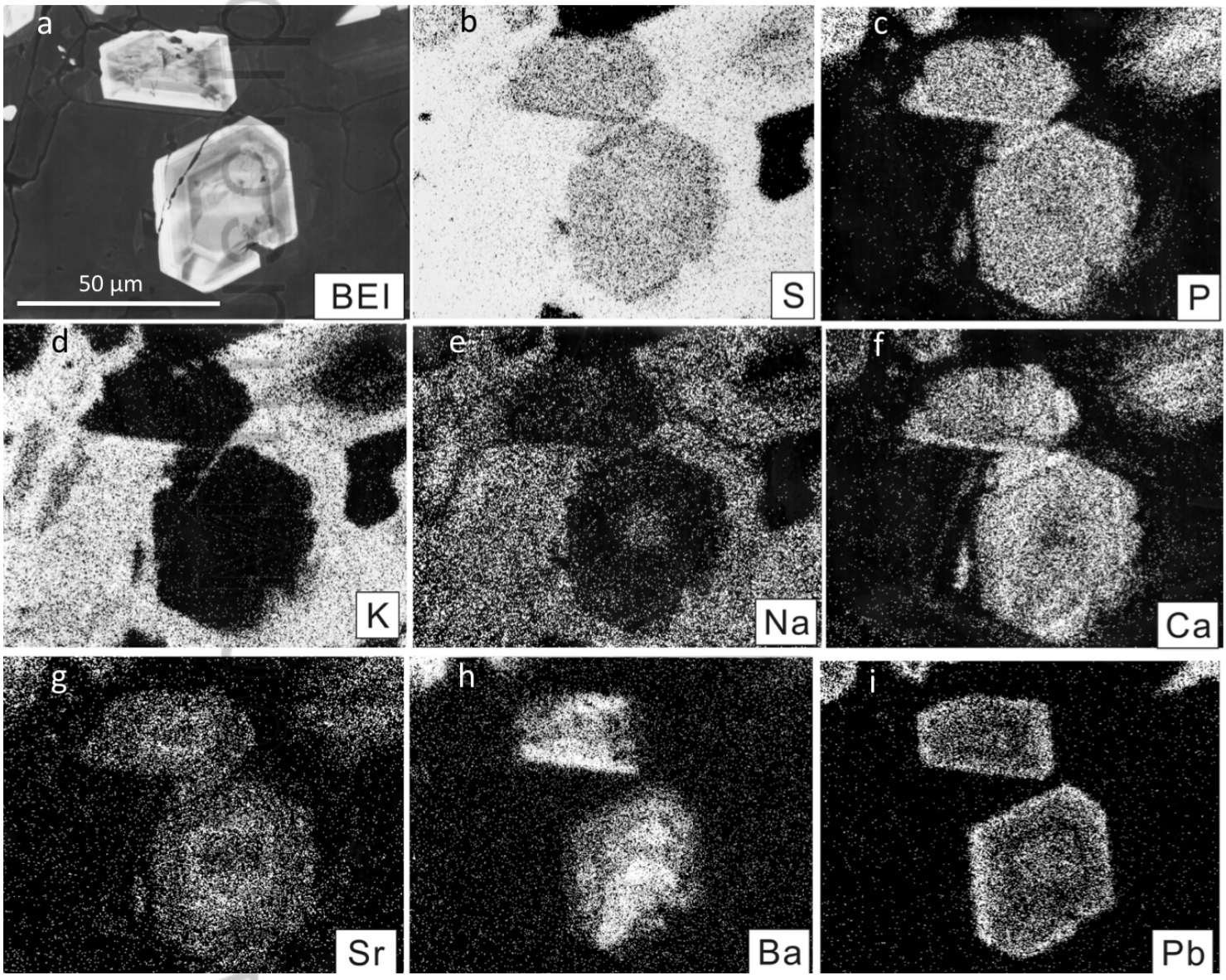

RGE_12127_F6.tiff

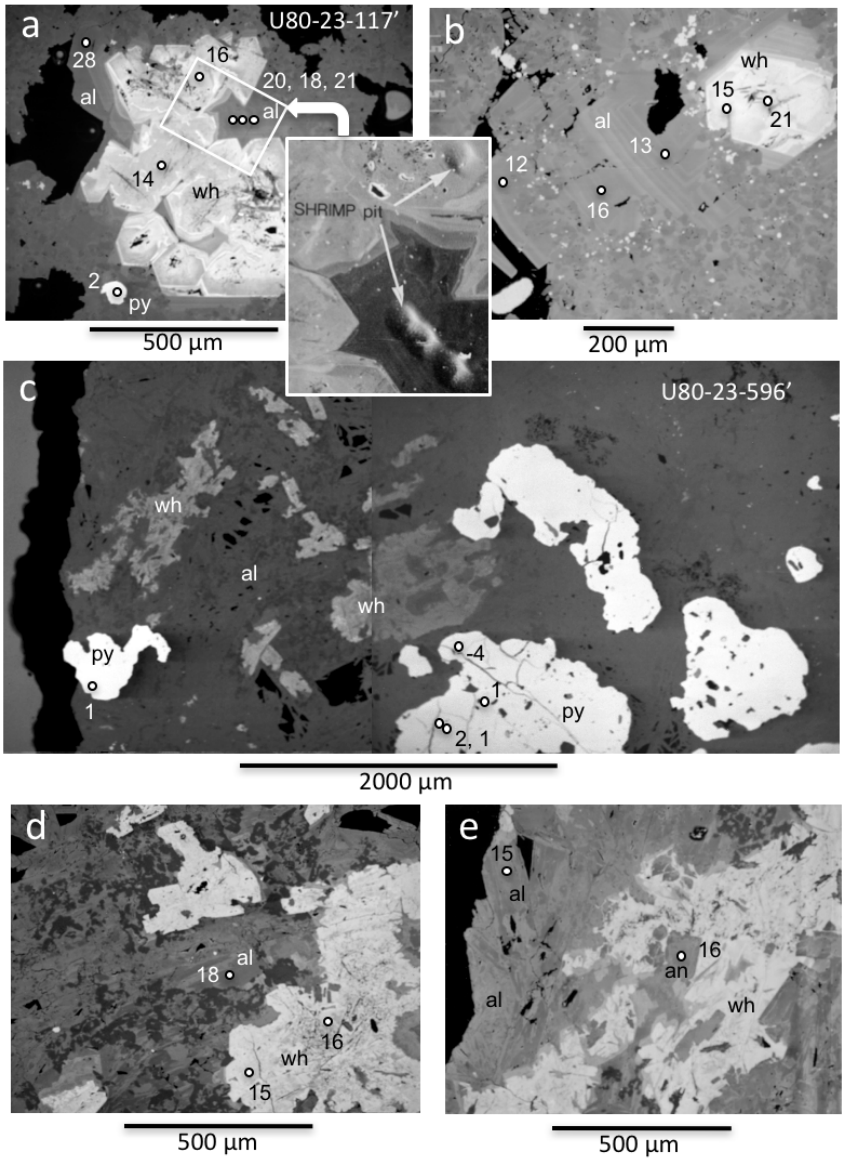

Fig. 7

RGE_12127_F7 .tiff

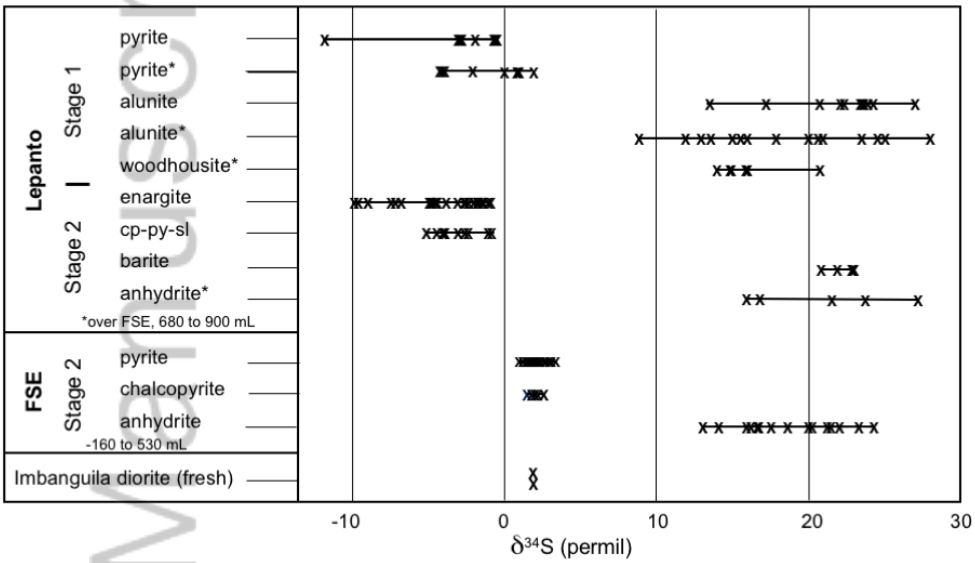

RGE_12127_F8.tiff

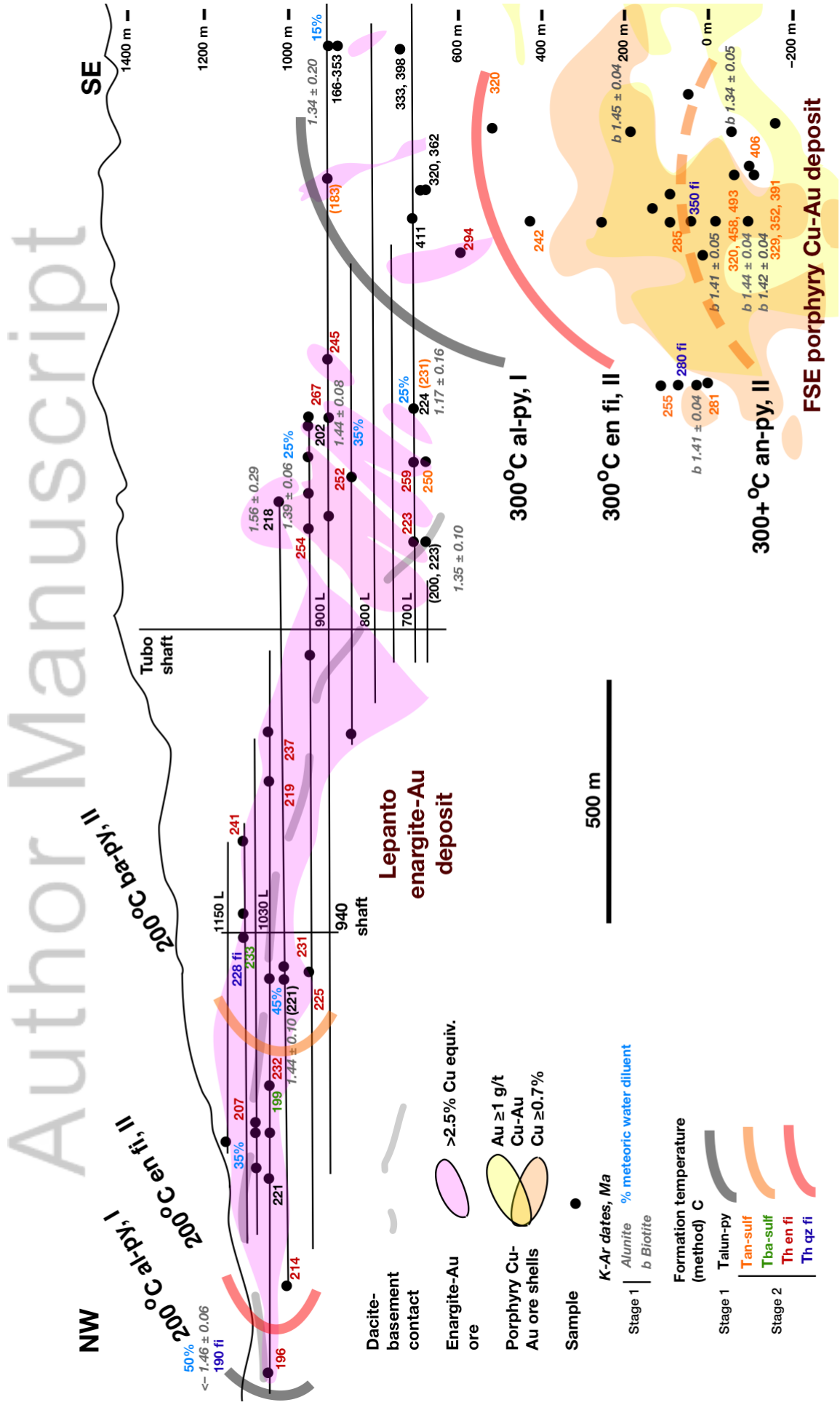

RGE_12127_F9.tiff